

REF ID: A219 193



**US Army Corps  
of Engineers**  
Construction Engineering  
Research Laboratory

USACERL Technical Manuscript E-90/01  
January 1990

2

AD-A219 193

# Multiple-Input Transfer Function Model of Heat Transfer From Square Slab Floors

by  
JoAnn Amber

DTIC  
ELECTE  
MAR 16 1990  
S D S D

Existing detailed hourly energy analysis programs do not adequately model the heat transfer between buildings and the ground. A simple model of the ground heat transfer compatible with both existing hourly energy analysis programs and simpler building models is vital as energy conservation techniques reduce the above-ground heat loss and building-ground heat transfer becomes more significant.

This study extends present techniques from the strictly geometric context of the numerical solution methods to the more conceptual environment of simplified models. Specifically, these concepts are applied to the problem of heat conduction through slab-on-grade surfaces.

Tested over a broad range of climatic conditions, the multiple-input transfer function model calculates slab heat flux. The accuracy of the model is dependent upon the accuracy of the input data; however, some reasonable approximations to the necessary input data can give acceptable results.

The full capability of the model was not tested in this study. Further work to develop a definition of the network parameters based on characteristic length could expand the use of the model to nonsquare and possibly even nonrectangular surfaces.

Approved for public release; distribution is unlimited.

90 03 15 016

The contents of this report are not to be used for advertising, publication, or promotional purposes. Citation of trade names does not constitute an official indorsement or approval of the use of such commercial products. The findings of this report are not to be construed as an official Department of the Army position, unless so designated by other authorized documents.

***DESTROY THIS REPORT WHEN IT IS NO LONGER NEEDED***

***DO NOT RETURN IT TO THE ORIGINATOR***

UNCLASSIFIED

SECURITY CLASSIFICATION OF THIS PAGE

REPORT DOCUMENTATION PAGE				Form Approved OMB No 0704 0188 Exp Date Jun 30 1986	
1a REPORT SECURITY CLASSIFICATION UNCLASSIFIED			1b RESTRICTIVE MARKINGS		
2a SECURITY CLASSIFICATION AUTHORITY			3 DISTRIBUTION / AVAILABILITY OF REPORT Approved for public release; distribution is unlimited.		
2b DECLASSIFICATION / DOWNGRADING SCHEDULE					
4 PERFORMING ORGANIZATION REPORT NUMBER(S) USACERL Technical Manuscript E-90/01			5 MONITORING ORGANIZATION REPORT NUMBER(S)		
6a NAME OF PERFORMING ORGANIZATION U.S. Army Construction Engr Research Laboratory		6b OFFICE SYMBOL (If applicable) CECER-ES	7a NAME OF MONITORING ORGANIZATION		
6c ADDRESS (City, State, and ZIP Code) P.O. Box 4005 Champaign, IL 61824-4005			7b ADDRESS (City, State, and ZIP Code)		
8a NAME OF FUNDING / SPONSORING ORGANIZATION HQUSACE		8b OFFICE SYMBOL (If applicable)	9 PROCUREMENT INSTRUMENT IDENTIFICATION NUMBER		
3c ADDRESS (City, State, and ZIP Code) 20 Massachusetts Avenue, NW. Washington, DC 20314-1000			10 SOURCE OF FUNDING NUMBERS		
			PROGRAM ELEMENT NO 4A161102	PROJECT NO AT23	TASK NO EB
					WORK UNIT ACCESSION NO ER9
11 TITLE (Include Security Classification) Multiple-Input Transfer Function Model of Heat Transfer From Square Slab Floors (U)					
12 PERSONAL AUTHOR(S) Amber, Joann					
13a TYPE OF REPORT Final		13b TIME COVERED FROM _____ TO _____		14 DATE OF REPORT (Year, Month, Day) 1990, January	
15 PAGE COUNT 123					
16 SUPPLEMENTARY NOTATION Copies are available from the National Technical Information Service, 5285 Port Royal Road, Springfield, VA 22161.					
17 COSATI CODES			18 SUBJECT TERMS (Continue on reverse if necessary and identify by block number)		
FIELD	GROUP	SUB-GROUP	heat transfer square slab floors		
20	13		buildings		
10	01		ground		
19 ABSTRACT (Continue on reverse if necessary and identify by block number)					
<p>Existing detailed hourly energy analysis programs do not adequately model the heat transfer between buildings and the ground. A simple model of the ground heat transfer compatible with both existing hourly energy analysis programs and simpler building models is vital as energy conservation techniques reduce the above-ground heat loss and building-ground heat transfer becomes more significant.</p> <p>This study extends present techniques from the strictly geometric context of the numerical solution methods to the more conceptual environment of simplified models. Specifically, these concepts are applied to the problem of heat conduction through slab-on-grade surfaces.</p>					
(Cont'd)					
20 DISTRIBUTION / AVAILABILITY OF ABSTRACT <input type="checkbox"/> UNCLASSIFIED / UNLIMITED <input checked="" type="checkbox"/> SAME AS RPT <input type="checkbox"/> DTIC USERS			21 ABSTRACT SECURITY CLASSIFICATION UNCLASSIFIED		
22a NAME OF RESPONSIBLE INDIVIDUAL Linda L. Wheatley			22b TELEPHONE (Include Area Code) (217) 352-6511 (ext 338)		22c OFFICE SYMBOL CECER-IMT

UNCLASSIFIED

BLOCK 19. (Cont'd)

Tested over a broad range of climatic conditions, the multiple-input transfer function model calculates slab heat flux. The accuracy of the model is dependent upon the accuracy of the input data; however, some reasonable approximations to the necessary input data can give acceptable results.

The full capability of the model was not tested in this study. Further work to develop a definition of the network parameters based on characteristic length could expand the use of the model to non-square and possibly even nonrectangular surfaces.

UNCLASSIFIED

## FOREWORD

This research was funded under Project 4A161102AT23, "Basic Research in Military Construction"; Work Unit EB-ER9, "Underground Heat Transfer Algorithms."

This manuscript was submitted in partial fulfillment of the requirements for the degree of Master of Science in Mechanical Engineering in the Graduate College of the University of Illinois at Urbana-Champaign. The advisor for this thesis was Dr. Curt Pedersen.

Technical guidance and support were provided by Dr. William P. Bahnfleth and Linda Lawrie, Energy Systems Division (ES), USACERL. Dr. Gilbert R. Williamson is Chief of USACERL-ES.

COL Carl O. Magnell is Commander and Director of USACERL, and Dr. L. R. Shaffer is Technical Director.

Accession For	
NTIS	DTIC
DTIC	DTIC
DTIC	DTIC
DTIC	DTIC
B,	
Distribution	
Dist	
A-1	



# CONTENTS

	Page
DD FORM 1473	iii
FOREWORD	v
LIST OF FIGURES	vii
LIST OF TABLES	ix
1 INTRODUCTION .....	1
2 CONCEPT .....	2
3 MODEL DEVELOPMENT .....	5
Structure	5
Basic Equations	6
Geometry	11
Soil Properties	16
Inputs	17
4 NETWORK .....	18
Method	18
Base Case	18
Description of Test System	19
Geometric Definition of Network Parameters	24
Parameter Refinement Using Empirical Methods	34
5 FINAL DEFINITION AND TESTING .....	52
Final Definition	52
Validation	57
6 NETWORK PARAMETERS BASED ON CHARACTERISTIC LENGTH ....	78
7 UTILIZATION OF THE GTF MODEL FOR ENERGY ANALYSIS .....	87
8 CONCLUSIONS .....	88
9 REFERENCES .....	89
APPENDIX A: SEEM'S METHOD	90
APPENDIX B: TRUE BASIC PROGRAM GTF	96
APPENDIX C: TRUBASIC PROGRAM QCALC	108
DISTRIBUTION	

# LIST OF FIGURES

Figure Number		Page
1	7-Node Network Model .....	5
2	Undisturbed Ground Temperature Profiles .....	13
3	FDM of Two Square Slabs .....	19
4	Daily Average Air Temperature - Minneapolis MN...	22
5	Daily Average Air Temperature - Medford OR .....	22
6	Daily Average Air Temperature - Philadelphia PA .	23
7	Daily Average Air Temperature - Phoenix AZ .....	23
8	Flux -- FDM and Run 1A .....	33
9	Flux and Difference -- Run 1A .....	33
10	Flux -- FDM and Run 1B .....	36
11	Flux and Difference -- Run 1B .....	36
12	Flux -- FDM and Run 1C .....	38
13	Flux and Difference -- Run 1C .....	39
14	Flux and Difference -- Run 2A .....	41
15	Flux and Difference -- Run 2B .....	44
16	Flux and Difference -- Run 2C .....	46
17	Flux and Difference -- Run 2D .....	48
18	Flux and Difference -- Minneapolis MN .....	58
19	Flux and Difference -- Medford OR .....	58
20	Flux and Difference -- Philadelphia PA .....	59
21	Flux and Difference -- Phoenix AZ .....	59
22	Flux and Difference -- 6 X 24 Rectangle .....	61

Figure Number		Page
23	Flux and Difference -- 18 X 112 Rectangle .....	62
24	Flux and Difference -- Tf=Toa -- Minneapolis MN .	67
25	Flux and Difference -- Tf=Toa -- Medford OR .....	67
26	Flux and Difference -- Tf=Toa -- Philadelphia PA	68
27	Flux and Difference -- Tf=Toa -- Phoenix AZ .....	68
28	Flux and Difference -- Tf=Toa -- 45 X 45 -- Minneapolis MN .....	69
29	Flux and Difference -- Td = Annual Mean Toa -- Minneapolis MN .....	71
30	Flux and Difference -- Td = Annual Mean Toa -- Medford OR .....	71
31	Flux and Difference -- Td = Annual Mean Toa -- Philadelphia PA .....	72
32	Flux and Difference -- Td = Annual Mean Toa -- Phoenix AZ .....	72
33	Flux and Difference -- Td = Annual Mean Toa -- 45 X 45 -- Minneapolis MN .....	73
34	Flux and Difference -- Tb=Tia -- Minneapolis MN .	75
35	Flux and Difference -- Tb=Tia -- Medford OR .....	75
36	Flux and Difference -- Tb=Tia -- Philadelphia PA	76
37	Flux and Difference -- Tb=Tia -- Phoenix AZ .....	76
38	Flux and Difference -- Tb=Tia -- 45 X 45 -- Minneapolis MN .....	77
39	Flux and Difference -- Run 3A .....	84
40	Flux and Difference -- Run 3B .....	84
41	Flux and Difference -- Run 3C .....	85
42	Flux and Difference -- Run 3D .....	85

# LIST OF TABLES

Table Number		Page
1	Parameter Sets for 1A - 1C .....	35
2	Results of Runs 1A - 1C .....	39
3	Parameter Sets for Runs 2A - 2D .....	40
4	Results of Runs 2A and 2B .....	43
5	Results of Runs 2A - 2D .....	48
6	Parameter Sets for Runs 1A - 1D .....	50
7	Results of Runs 1A - 1D .....	51
8	Results of GTF Models for Various Locations ....	60
9	Results of GTF Models for Non-square Slabs .....	62
10	Results of Substituting Daily Average Outdoor Air Temperature for Daily Average Ground Surface Temperature .....	66
11	Results of Substituting Annual Average Air Temperature for Annual Average Ground Surface Temperature .....	70
12	Results of Substituting Constant Indoor Air Temperature for Daily Average Slab Surface Temperature .....	74
13	Parameter Sets for Empirical Models .....	80
14	Equations of Lines Fit to Empirical Data .....	81
15	Equations of Common Lines Fit to Empirical Data	82
16	Parameter Sets Calculated Using Empirical Equations .....	83
17	Results of GTF Model Using Parameter Sets Based on Empirical Equations .....	86

# MULTIPLE-INPUT TRANSFER FUNCTION MODEL OF HEAT TRANSFER FROM SQUARE SLAB FLOORS

## 1 INTRODUCTION

Existing detailed hourly energy analysis programs such as BLAST<sup>\*</sup> do not adequately model the heat transfer between buildings and the ground. Although the model of the building can be very complex, the models of the building-ground heat transfer mechanisms are generally incongruously simple. BLAST, for example, uses a one-dimensional response factor model with a single monthly average ground temperature to define all building-ground heat transfer. A simple model of the ground heat transfer compatible with both existing hourly energy analysis programs and simpler building models becomes more vital as energy conservation techniques reduce the above-ground heat loss and building-ground heat transfer becomes more significant.

Ceylan and Myers [1] developed a response-coefficient method for multidimensional heat conduction problems which is substantially more efficient than finite-difference or finite-element methods. Additionally, it provides a response coefficient model of the system which can be used with any input data which can be approximated by a continuous, piecewise linear function. Seem [2] developed a procedure for calculating multidimensional transfer functions which eliminates some of the computationally expensive steps of the Ceylan and Myers method. These multidimensional methods have been applied to strictly geometric heat conduction problems. The objective of this study is to extend these techniques from the strictly geometric context of the numerical solution methods to the more conceptual environment of simplified models. Specifically, these concepts will be applied to the problem of heat conduction through slab-on-grade surfaces.

---

<sup>\*</sup>Building Load Analysis and System Thermodynamics (BLAST) was developed by USACERL and funded through the Department of Defense for military construction projects.

## 2 CONCEPT

Many physical systems, including thermodynamic systems, can be approximated using lumped-system analysis. In this approach the system is described as a series of lumped, linear, dynamic elements defined by ordinary differential equations. The network analogy provides a simple visualization of this concept. In a network model of a thermal system, temperatures are represented by nodes with a linear temperature distribution between each pair of nodes. Physical properties are considered to be uniform between each pair of nodes, but can vary from pair to pair. Energy balance equations are written for each node and the system of equations solved for unknown temperatures and heat fluxes. The validity of the system model is dependent on the accuracy of the assumptions of uniform temperature at each node and linearity between nodes.

Without defining specific geometric or environmental properties, the matrices forming the energy balance equations of the nodes are constructed using state space representation resulting in the state equation

$$\frac{\partial X}{\partial t} = AX + BU \quad (1)$$

and the output equation

$$Q = CX + DU \quad (2)$$

The matrix  $X$  contains the unknown temperatures (state variables).  $U$  is the matrix of known temperatures (input

variables).  $Q$  is the matrix of fluxes (output variables). Matrices  $A$ ,  $B$ ,  $C$ , and  $D$  are coefficient matrices. The size of the matrices and the values of the elements will be determined by the specific model. Once the coefficient matrices are defined and the input values identified, the first order differential equations can be solved. The method of Seem [2] is used to solve the system of equations. In this formulation, the time series of input variables is modelled as a continuous piecewise linear function by the equation

$$U(\tau) = U_t + \frac{(\tau - t)}{\delta} (U_{t+\delta} - U_t) \quad (3)$$

Using this function for the inputs, the differential equations are solved, and substituted for  $X$  into the equation (2) resulting in an equation relating the system outputs to the system inputs. This equation is known as the transfer function equation and is of the form

$$Q_t = \sum_{j=0}^n (S_j U_{t-j\delta}) - \sum_{j=0}^n (e_j Q_{t-j\delta}) \quad (4)$$

where

$Q_t$  = vector of output variables (heat flux) at time  $i$

$S_j$  = transfer function matrix for temperature inputs  
at time  $j$

$j$  = designator identifying a point in time, where  $j=0$  is the current time,  $j=1$  is one time step prior to the current time and so on

$t$  = time of interest

$\delta$  = time step

$U_i$  = vector of input variables (known temperatures)  
at time  $i$

$e$  = scalar constant for adjusting the effect of previous  
outputs on the output at the time of interest.

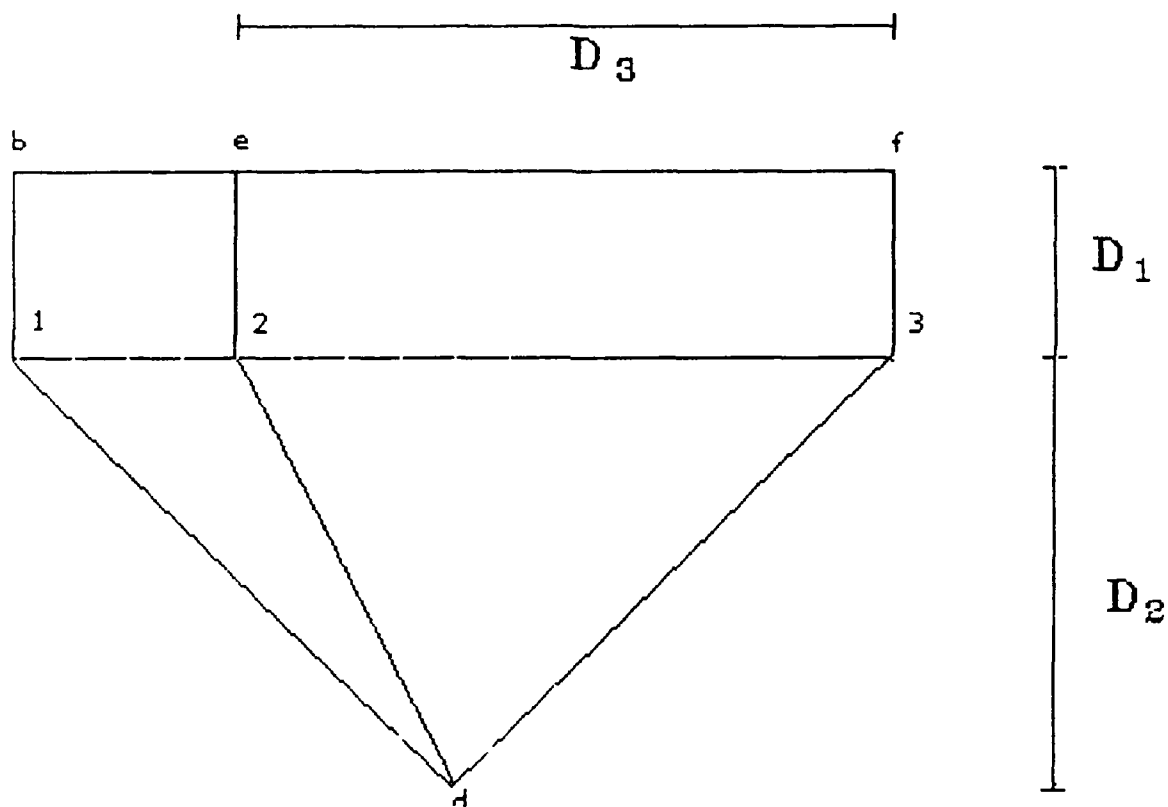
A transfer function is defined as the ratio of the output variables of a system in state space to its input variables (also in state space). In this way, the transfer function represents the dynamics of a linear time-invariant system. The transfer function matrices are dependent on the system and inputs, but only on the functional form of the inputs; therefore, any input which can be adequately modelled by the continuous piecewise linear function noted above can be used with the transfer function matrices to model its effect on the system. This is particularly useful in the modelling of building systems where the input conditions of climate are unpredictable and highly variant in time and geographic location.

### 3 MODEL DEVELOPMENT

#### 3.1 STRUCTURE

The system modelled for this study is a square slab-on-grade. The model proposed is a 7 node network with 3 state variables and 4 inputs [Figure 1].

Figure 1: 7 Node Network Model



The known temperatures (or inputs) are the daily average slab core region temperature ( $T_b$ ), the daily average slab

edge region temperature ( $T_e$ ), the daily average ground surface temperature ( $T_f$ ) and the deep ground temperature ( $T_d$ ). The 3 state variables, the temperatures at the remaining nodes ( $T_1, T_2, T_3$ ), are allowed to float and consequently have some thermal capacitance attributed to them. The temperature nodes are related to each other as shown in the figure. Between attached pairs of temperature nodes, there exists some thermal resistance. The definition of these resistances and capacitances is discussed in Section 3.2.

### 3.2 BASIC EQUATIONS

**BASIC EQUATIONS** Energy balance equations are written for each node resulting in 4 state equations of the form

$$C_i \frac{\partial T_i}{\partial t} = \sum_{j=1}^4 G_{ji} (T_j - T_i) \quad (5)$$

for  $i = 1$  to 4, and 3 state output equations of the form

$$Q_i = \sum_{j=1}^4 G_{ji} (T_j - T_i) \quad (6)$$

for  $i = 1$  to 3, where

$C_i$  = thermal capacitance at node  $T_i$

$G_{ji} = \frac{1}{R_{ji}}$  = inverse of the thermal resistance between

nodes  $T_j$  and  $T_i$

These 7 equations can be written more conveniently in matrix form

$$\frac{\partial \lambda}{\partial t} = \mathcal{A}X + \mathcal{B}U \quad (7)$$

and

$$Q = C X + \mathcal{D} U \quad (8)$$

where

$$\frac{\partial X}{\partial t} = \begin{pmatrix} \frac{\partial T_1}{\partial t} \\ \frac{\partial T_2}{\partial t} \\ \frac{\partial T_3}{\partial t} \end{pmatrix} \quad (9)$$

$$X = \begin{pmatrix} T_1 \\ T_2 \\ T_3 \end{pmatrix} \quad (10)$$

$$U = \begin{pmatrix} T_b \\ T_f \\ T_d \\ T_e \end{pmatrix} \quad (11)$$

$$Q = \begin{pmatrix} Q_b \\ Q_f \\ Q_d \\ Q_e \end{pmatrix} \quad (12)$$

$$A = \begin{pmatrix} \frac{-G_{1b} - G_{12} - G_{1d}}{C_1} & \frac{G_{12}}{C_1} & 0 \\ \frac{G_{12}}{C_2} & \frac{-G_{2e} - G_{12} - G_{23} - G_{2d}}{C_2} & \frac{G_{23}}{C_2} \\ 0 & \frac{G_{23}}{C_3} & \frac{-G_{3f} - G_{23} - G_{3d}}{C_3} \end{pmatrix} \quad (13)$$

$$B = \begin{pmatrix} \frac{G_{1b}}{C_1} & 0 & \frac{G_{1d}}{C_1} & 0 \\ 0 & 0 & \frac{G_{2d}}{C_2} & \frac{G_{2e}}{C_2} \\ 0 & \frac{G_{3f}}{C_3} & \frac{G_{3d}}{C_3} & 0 \end{pmatrix} \quad (14)$$

$$C = \begin{pmatrix} G_{1b} & 0 & 0 \\ 0 & 0 & G_{3f} \\ G_{1d} & G_{2d} & G_{3d} \\ 0 & G_{2e} & 0 \end{pmatrix} \quad (15)$$

$$D = \begin{pmatrix} -G_{1b} - G_{be} & 0 & 0 & G_{be} \\ 0 & -G_{3f} - G_{ef} & 0 & G_{ef} \\ 0 & 0 & -G_{1d} - G_{2d} - G_{3d} & 0 \\ G_{be} & G_{ef} & 0 & -G_{be} - G_{ef} - G_{2e} \end{pmatrix} \quad (16)$$

The coefficient matrices A, B, C, and D define the relationships of all temperature regions in the system to all others. They involve geometric factors such as the area through which heat is transferred from one region to another, and physical properties such as the density and thermal conductivity of various regions. The goal of defining the elements of the coefficient matrices is to make it possible to generate transfer function equations for any system from its basic physical parameters rather than as is frequently done in electro-mechanical systems - by testing

the system itself. Because the important aspect of the equations is the thermal relationships between regions, the model is not strictly geometric.

The first step in defining the matrix coefficients is identifying the properties which make up the elements of  $G$  and  $C$ . The basic form allows for the description of several heat transfer mechanisms given the appropriate temperatures. For conduction, the equation becomes

$$Q = kA \frac{\partial T}{\partial x} \quad (17)$$

or, in the spatially discretized form used for this model

$$Q_{ij} = \left( \frac{k_{ij} A_{ij}}{L_{ij}} \right) (T_i - T_j). \quad (18)$$

In this case  $G_{ij}$  is defined as the conductance,  $\frac{kA}{L}$ , where

$k_{ij}$  = thermal conductivity applicable to the volume  
between nodes  $i$  and  $j$

$A_{ij}$  = cross-sectional area through which heat is transferred between nodes  $i$  and  $j$

$L_{ij}$  = distance between nodes  $i$  and  $j$ .

Although this model does not contain convective or radiative heat transfer, these mechanisms can be supported by the model by setting

$$G = h A \quad (19)$$

for convective heat transfer, and

$$G = h_r A \quad (20)$$

for radiative heat transfer, where

$h$  = convective heat transfer coefficient

and

$h_r$  = the effective linearized radiative heat transfer coefficient.

The thermal capacitance  $C$  is derived from the transient equation

$$Q = \rho c_p V \frac{\partial T}{\partial t} \quad (21)$$

so that

$$C_i = \rho_i c_{p_i} V_i \quad (22)$$

where

$\rho_i$  = density of the region of soil at  $T_i$

$c_{p_i}$  = specific heat of the region of soil at  $T_i$

$V_i$  = volume of the region of soil at  $T_i$ .

Both thermal conductance,  $G_{ij}$ , and thermal capacitance,  $C_i$ , are composed of geometric factors ( $L_{ij}$ ,  $A_{ij}$ , and  $V_i$ ) as well as soil properties ( $k_{ij}$ ,  $\rho_i$ , and  $c_{pi}$ ). These will be discussed separately.

### 3.3 GEOMETRY

Bahnfleth's study of undisturbed ground temperature patterns [3] shows two distinctly different zones of temperature fluctuation: a relatively fast zone near the ground surface where the temperature changes are in scale with the temperature changes of the forcing temperature, and a slower zone where temperature fluctuations are strongly damped. Because the response rate of the near-surface zone is more similar to the response rate of typical building components than to that of the remainder of the earth, it was decided to model the near-surface earth and the remainder of the earth as attached but distinct components. The point of separation of these zones is the diurnal penetration depth, or roughly 0.5 meters below the surface. The temperature at this point remains nearly constant over a day at the daily average ground surface temperature.

Horizontal maps of ground temperature beneath buildings show a circular pattern, consequently, a cylindrical coordinate system was used to produce an axisymmetric two-dimensional model. Horizontal temperature nodes are set at the slab center, the edge-equivalent radius, and the location where the ground temperature is unaffected by the building (far-field). The edge-equivalent radius is calculated as the radius of a circle of equivalent slab perimeter, or

$$r_p = \frac{P}{2\pi}. \quad (23)$$

In this fashion, a 10m by 10m slab is mapped to a circle of radius

$$r_p = \frac{40}{2\pi} = 6.37m \quad (24)$$

Vertical temperature nodes are set at the diurnal penetration depth of the surface temperature wave (approximately 0.5m below the surface), the annual penetration depth (approximately 15m below the surface) and the depth of the point of inflection or knee of the undisturbed temperature profile (approximately 4m below the surface). Studies ([3], [4], [5]) of underground temperature patterns show a shape which could be approximated by linear temperature profiles between these temperature nodes (Figure 2).

The area-equivalent radius is used for calculations in the vertical plane. It is calculated as the radius of the circle which has the same area as the slab, i.e.

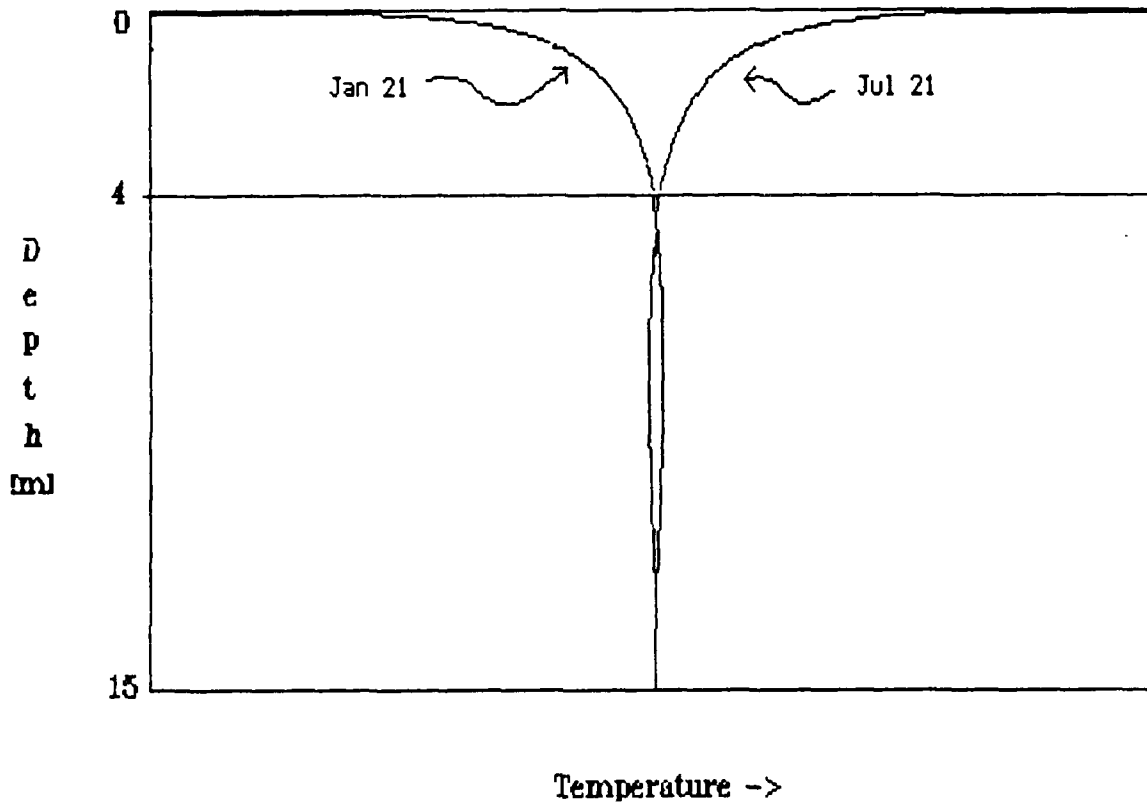
$$r_a = \sqrt{\frac{A}{\pi}}. \quad (25)$$

Therefore, for calculations in the vertical direction, the 10m by 10m slab is mapped to a circle of radius

$$r_a = \sqrt{\frac{100}{\pi}} = 5.64m \quad (26)$$

so that area is preserved.

Figure 2: Undisturbed Ground Temperature Profile



Although this model cannot be reproduced graphically, it accounts for both the perimeter and area effects of ground-coupled heat transfer.

These geometric relationships were used to build the geometric matrices which were used, in turn, to develop the coefficient matrices.

Three matrices constitute the geometric factors of the A, L, and V. Matrix A is the symmetric 7 x 7 matrix

$$A = \begin{pmatrix} A_{11} & A_{12} & A_{13} & A_{1b} & A_{1f} & A_{1d} & A_{1e} \\ A_{12} & A_{22} & A_{23} & A_{2b} & A_{2f} & A_{2d} & A_{2e} \\ A_{13} & A_{23} & A_{33} & A_{3b} & A_{3f} & A_{3d} & A_{3e} \\ A_{1b} & A_{2b} & A_{3b} & A_{bb} & A_{bf} & A_{bd} & A_{be} \\ A_{1f} & A_{2f} & A_{3f} & A_{bf} & A_{ff} & A_{fd} & A_{fe} \\ A_{1d} & A_{2d} & A_{3d} & A_{bd} & A_{fd} & A_{dd} & A_{de} \\ A_{1e} & A_{2e} & A_{3e} & A_{be} & A_{fe} & A_{de} & A_{ee} \end{pmatrix} \quad (27)$$

where the subscripts refer to the path, that is,  $A_{ij}$  is the area through which heat is transferred from  $T_i$  to  $T_j$ .

Matrix L is a similar symmetric 7 x 7 matrix:

$$L = \begin{pmatrix} L_{11} & L_{12} & L_{13} & L_{1b} & L_{1f} & L_{1d} & L_{1e} \\ L_{12} & L_{22} & L_{23} & L_{2b} & L_{2f} & L_{2d} & L_{2e} \\ L_{13} & L_{23} & L_{33} & L_{3b} & L_{3f} & L_{3d} & L_{3e} \\ L_{1b} & L_{2b} & L_{3b} & L_{bb} & L_{bf} & L_{bd} & L_{be} \\ L_{1f} & L_{2f} & L_{3f} & L_{bf} & L_{ff} & L_{fd} & L_{fe} \\ L_{1d} & L_{2d} & L_{3d} & L_{bd} & L_{fd} & L_{dd} & L_{de} \\ L_{1e} & L_{2e} & L_{3e} & L_{be} & L_{fe} & L_{de} & L_{ee} \end{pmatrix}. \quad (28)$$

For the 7 node network model, not all of the nodes are connected, therefore the elements which relate unconnected nodes to each other become 0 leaving

$$A = \begin{pmatrix} 0 & A_{12} & 0 & A_{1b} & 0 & A_{1d} & 0 \\ A_{12} & 0 & A_{23} & 0 & 0 & A_{2d} & A_{2e} \\ 0 & A_{23} & 0 & 0 & A_{3f} & A_{3d} & 0 \\ A_{1b} & 0 & 0 & 0 & 0 & 0 & A_{be} \\ 0 & 0 & A_{3f} & 0 & 0 & 0 & A_{fe} \\ A_{1d} & A_{2d} & A_{3d} & 0 & 0 & 0 & 0 \\ 0 & A_{2e} & 0 & A_{be} & A_{fe} & 0 & 0 \end{pmatrix} \quad (29)$$

and

$$L = \begin{pmatrix} 0 & L_{12} & 0 & L_{1b} & 0 & L_{1d} & 0 \\ L_{12} & 0 & L_{23} & 0 & 0 & L_{2d} & L_{2e} \\ 0 & L_{23} & 0 & 0 & L_{3f} & L_{3d} & 0 \\ L_{1b} & 0 & 0 & 0 & 0 & 0 & L_{be} \\ 0 & 0 & L_{3f} & 0 & 0 & 0 & L_{fe} \\ L_{1d} & L_{2d} & L_{3d} & 0 & 0 & 0 & 0 \\ 0 & L_{2e} & 0 & L_{be} & L_{fe} & 0 & 0 \end{pmatrix}. \quad (30)$$

$V$  is the vector

$$V = \begin{pmatrix} V_1 \\ V_2 \\ V_3 \end{pmatrix} \quad (31)$$

The definition of the elements, or network parameters,  $A_{ij}$ ,  $L_{ij}$ , and  $V_i$  is, in part, independent of the model structure, but is based on the geometry presented above and is described further in Section 4.

### 3.4 SOIL PROPERTIES

Soil properties are represented by another 7 x 7 symmetric matrix:

$$K = \begin{pmatrix} 0 & k_{12} & 0 & k_{1b} & 0 & k_{1d} & 0 \\ k_{12} & 0 & k_{23} & 0 & 0 & k_{2d} & k_{2e} \\ 0 & k_{23} & 0 & 0 & k_{3f} & k_{3d} & 0 \\ k_{1b} & 0 & 0 & 0 & 0 & 0 & k_{be} \\ 0 & 0 & k_{3f} & 0 & 0 & 0 & k_{fe} \\ k_{1d} & k_{2d} & k_{3d} & 0 & 0 & 0 & 0 \\ 0 & k_{2e} & 0 & k_{be} & k_{fe} & 0 & 0 \end{pmatrix} \quad (32)$$

and two vectors,

$$\rho = (\rho_1 \quad \rho_2 \quad \rho_3) \quad (33)$$

and

$$c_p = (c_{p1} \quad c_{p2} \quad c_{p3}). \quad (34)$$

Thermal properties of the soil can be defined separately for each energy balance equation. Individually, these equations assume constant thermal properties. Consequently, the properties are defined as the "effective" value of the thermal properties in the region specified by the equation. The need for an "effective" conductivity is described more thoroughly in Bahnfleth [3]. Effective conductivity is defined as

$$k_o = \frac{\sum l_k}{\sum \frac{l_k}{k_k}} \quad (35)$$

where

$l_k$  = the thickness of layer  $k$ , and

$k_k$  = the conductivity of layer  $k$ .

Calculated from this equation,  $k_{eff}$  is the effective value of the soil conductivity in the region through which heat transfers between  $T_i$  and  $T_j$ .

### 3.5 INPUTS

The inputs to the transfer function equation are (referring to Figure 1) the temperatures of the slab core area ( $T_b$ ) and the slab edge area ( $T_e$ ), and the undisturbed ground temperatures near the surface ( $T_s$ ) and in the deep ground ( $T_d$ ).

Because the "top" nodes are defined at the diurnal penetration depth, their temperatures can be approximated by the daily average of the surface temperature, i.e.  $T_b$  = the daily average slab center temperature and  $T_s$  = the daily average ground surface temperature. The undisturbed ground surface and deep ground temperatures can be determined a priori using a variety of algorithms.

## 4 NETWORK PARAMETER SPECIFICATION

### 4.1 METHOD

The network parameters are the elements which compose the geometric matrices  $A$ ,  $L$ , and  $V$ . Their definition depends on the method of discretizing the geometry of the system. In other words, the magnitude of the element is dependent on the sizes of the regions assumed to be at the specified temperatures. Because few of the regions are actually isothermal, the allocation of area and volume to a specific temperature must be based on some method or algorithm.

In order to evaluate the validity of the postulated network parameters a test system which fixes input conditions and environmental parameters was established. A base case using the same fixed conditions was used to compare both the total flux data and the form of the daily average flux curve. This provided not only data on the accuracy of the model but also clues to the nature of any inaccuracies that might occur.

### 4.2 BASE CASE

The baseline for evaluation of the model is a detailed finite difference model (FDM) of heat transfer from slab floors developed by Bahnfleth [3]. A three-dimensional model of a slab-on-grade and the soil beneath it is solved by numerical techniques in the program SLAB3D. The space above the slab is defined by a constant room air temperature. Undisturbed soil temperature distributions as calculated from subroutine TEARTH are used as the far-field

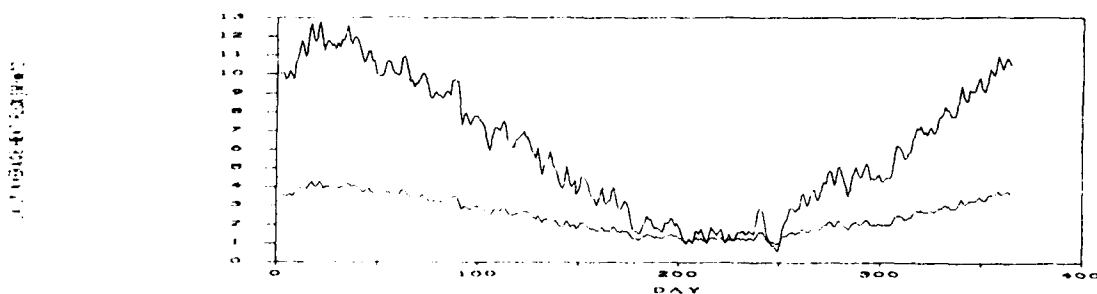
boundary temperatures. The deep ground boundary can be either a specified flux or a specified temperature plane. Bahnfleth generated data for a variety of surface shapes and sizes as well as a number of diverse climatic conditions.

#### 4.3 DESCRIPTION OF TEST SYSTEM

##### 4.3.1 GEOMETRY

Because the model was developed based on a square slab-on-grade, the development of the network parameters was based on this geometry. Base case data were available for two sizes of square slabs, a 12m x 12m square and a 45m x 45m square. The flux per unit area calculated by the finite difference model for these two slabs for a calendar year in Minneapolis MN is shown in Figure 3. Due to the dominance of the edge effect in the smaller slab, the annual flux variation is much greater for the smaller slab. If the effect of the balance between the perimeter loss and edge loss is to be accommodated, it is important that the test system strongly exhibits this effect. Consequently, the smaller 12m x 12m slab was used as the primary test system.

Figure 3: FDM of Two Square Slabs



#### 4.3.2 SOIL PROPERTIES

Although the system model can support variable soil properties, this capability is not tested in this study. Available base case heat flux data were calculated using constant soil properties. The same properties are used in this study. They are:

$$\rho = 1200 \text{ kg/m}^3$$

$$c_p = 1200 \text{ J/kg/K}$$

$$k = 1.00 \text{ W/m/K}$$

#### 4.3.3 INPUTS

For this study, existing data from Bahnfleth's one-dimensional semi-infinite solid model of the heat transfer in undisturbed earth [3] were used to provide input data for the nodes at the far-field and the deep ground. The hourly ground surface temperatures calculated by this model vary with local climatic conditions while the deep ground temperature is constant at the annual average ground surface temperature. Because the far-field node is placed at the diurnal penetration depth, the daily average ground surface temperature rather than the hourly ground surface temperature is used as input to the multiple input transfer function model.

Exact data for the daily average slab center and slab edge temperatures were not available from the base case data set. This is the usual case with most energy analysis programs. Therefore, although it is possible in the network mode to include a temperature difference between the slab center and the slab edge, daily average slab surface temperatures (which are equal to the ground temperature at the diurnal penetration depth) were used for both these temperatures. The network parameters developed using the assumption of an isothermal slab should be appropriate for use with energy analysis programs, such as BLAST and DOE-2 which use the same assumption.

Data were available from the base case data set for four locations, Minneapolis MN, Medford OR, Philadelphia PA, and Phoenix AZ. These data were generated originally from Typical Meteorological Year (TMY) weather data for these sites. Figures 4, 5, 6, 7 show the daily average air temperatures at these four locations.

In order to develop the most responsive model network parameters, the most rigorous weather conditions were used. The figures indicate that the weather data for Minneapolis MN would provide the most demanding conditions for the model. In addition to a large annual temperature variation, the temperature variation from day to day is also larger in the Minneapolis data than in that of the other three locations. During the development of the network parameters, therefore, the data derived using Minneapolis weather were utilized to evaluate the accuracy of the model fit. The model was then tested later at the remaining three locations.

Figure 4: Daily Average Air Temperature -- Minneapolis MN

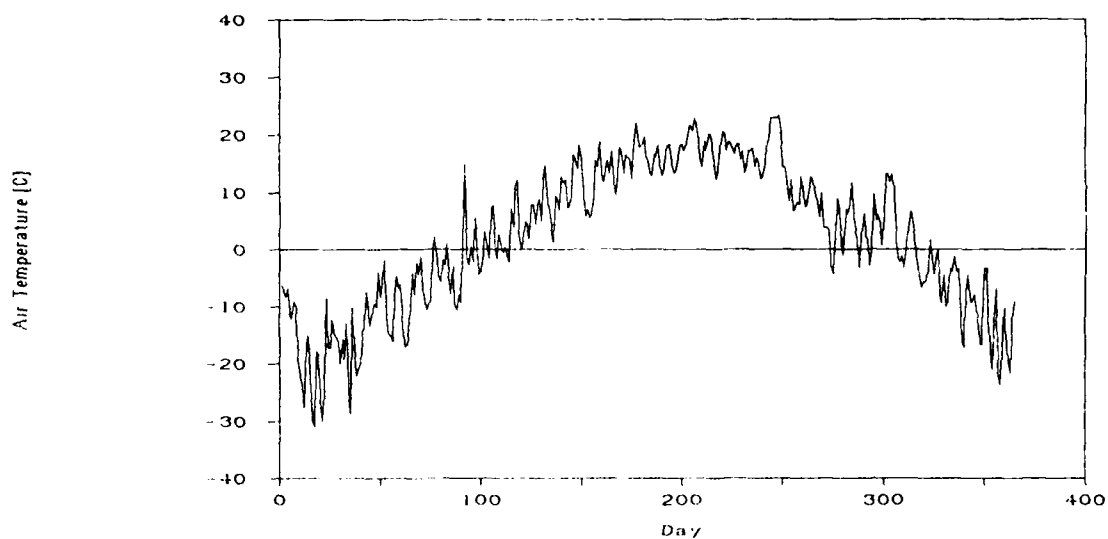


Figure 5: Daily Average Air Temperature -- Medford OR

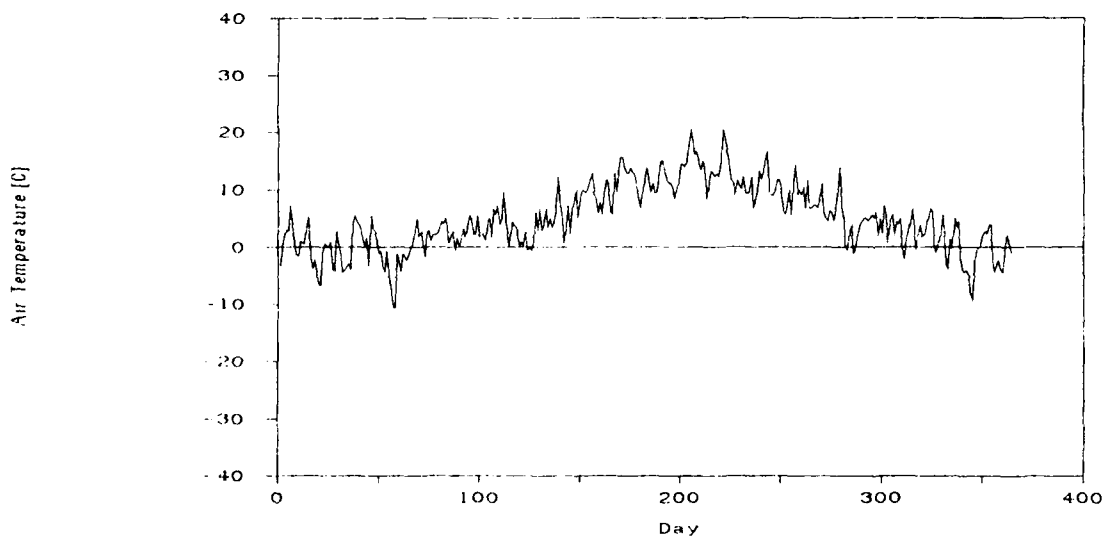


Figure 6: Daily Average Air Temperature -- Philadelphia PA

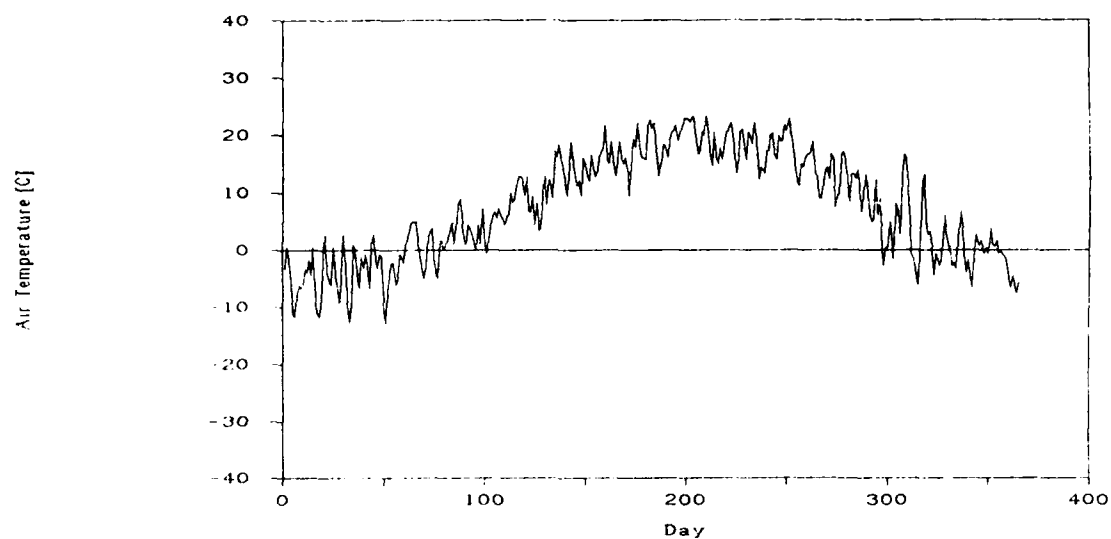
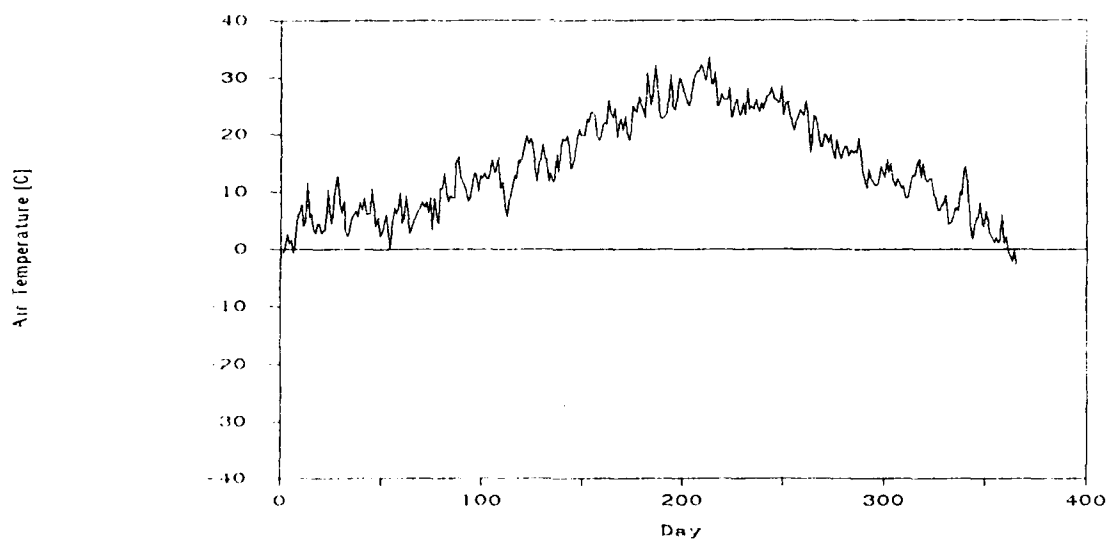


Figure 7: Daily Average Air Temperature -- Phoenix AZ



#### 4.4 GEOMETRIC DEFINITION OF NETWORK PARAMETERS

The geometric definition of the network parameters is based on a series of assumptions about the size and shape of the temperature regions beneath the slab as well as the geometry of the slab itself. The geometry of the slab and the ground in the vicinity of the slab is the foundation for these assumptions. For the test system, the slab geometry is defined by

$$A_s = 12 \times 12 = 144 \text{ m}^2 \quad (36)$$

$$P_s = 4 \times 12 = 48 \text{ m}$$

$$r_a = \sqrt{\frac{A_s}{\pi}} = 6.77 \text{ m}$$

$$r_p = \frac{P_s}{2\pi} = 7.64 \text{ m}.$$

The ground geometry has already been fixed by the network model [see Figure 1].

The elements  $L_{ij}$  of the matrix  $L$  can then be assigned as the distance between nodes  $i$  and  $j$ , that is,

$$L = \begin{pmatrix} 0 & L_{12} & 0 & L_{1b} & 0 & L_{1d} & 0 \\ L_{12} & 0 & L_{23} & 0 & 0 & L_{2d} & L_{2e} \\ 0 & L_{23} & 0 & 0 & L_{3f} & L_{3d} & 0 \\ L_{1b} & 0 & 0 & 0 & 0 & 0 & L_{be} \\ 0 & 0 & L_{3f} & 0 & 0 & 0 & L_{fe} \\ L_{1d} & L_{2d} & L_{3d} & 0 & 0 & 0 & 0 \\ 0 & L_{2e} & 0 & L_{be} & L_{fe} & 0 & 0 \end{pmatrix}. \quad (37)$$

Referring to Figure 1, note that

$$L_{1b} = L_{2e} = L_{3f} = D_1 \quad (38)$$

$$L_{1d} = L_{2d} = L_{3d} = D_2 \quad (39)$$

$$L_{fe} = L_{23} = D_3 \quad (40)$$

and

$$L_{be} = L_{12} = r_p. \quad (41)$$

Substituting  $D_1$ ,  $D_2$ ,  $D_3$ , and  $r_p$  into  $L$ ,

$$L = \begin{pmatrix} 0 & r_p & 0 & D_1 & 0 & D_2 & 0 \\ r_p & 0 & D_3 & 0 & 0 & D_2 & D_1 \\ 0 & D_3 & 0 & 0 & D_1 & D_2 & 0 \\ D_1 & 0 & 0 & 0 & 0 & 0 & r_p \\ 0 & 0 & D_1 & 0 & 0 & 0 & D_3 \\ D_2 & D_2 & D_2 & 0 & 0 & 0 & 0 \\ 0 & D_1 & 0 & r_p & D_3 & 0 & 0 \end{pmatrix}. \quad (42)$$

The elements of  $A$  are defined as the area through which heat is transferred between  $T_i$  and  $T_j$ ,

$$A = \begin{pmatrix} 0 & A_{12} & 0 & A_{1b} & 0 & A_{1d} & 0 \\ A_{12} & 0 & A_{23} & 0 & 0 & A_{2d} & A_{2e} \\ 0 & A_{23} & 0 & 0 & A_{3f} & A_{3d} & 0 \\ A_{1b} & 0 & 0 & 0 & 0 & 0 & A_{be} \\ 0 & 0 & A_{3f} & 0 & 0 & 0 & A_{fe} \\ A_{1d} & A_{2d} & A_{3d} & 0 & 0 & 0 & 0 \\ 0 & A_{2e} & 0 & A_{be} & A_{fe} & 0 & 0 \end{pmatrix} \quad (43)$$

The determination of the elements of  $A$  is more complex than the determination of the elements of  $L$ . Although the model is not strictly geometric, the heat transfer areas can be initially postulated based on geometric considerations. First, it is assumed that  $A_{1b} = A_{1d}$ ,  $A_{2e} = A_{2d}$ , and  $A_{3f} = A_{3d}$ . Then the area through which heat is transferred between  $T_b$  and  $T_1$  can be estimated by the area of the slab which can be approximated by the daily average slab surface center temperature,  $T_b$ . Studies [3],[4], and [5] have shown that temperature gradients across horizontal ground-contact surfaces are small over most of the surface and relatively large near the edge. For this model the area in the plane of the ground surface considered to be at  $T_b$  is the area of the slab minus the area near the slab edge, or

$$A_{1b} = A_{1d} = \pi(r_a - d_1)^2 \quad (44)$$

where  $d_1$  is the distance from the slab edge to the location where the slab surface temperature is approximately  $T_b$ .

The area through which heat is transferred between  $T_e$  and  $T_2$  can be defined as the area where the edge effect predominates. This area is specified as the area within a definable distance,  $d_2$  of the building edge minus the area already associated with  $T_b$ , or

$$A_{2e} = A_{2d} = \pi(r_a + d_2)^2 - A_{1b} \quad (45)$$

where  $d_2$  is the distance the edge effect region extends beyond the slab edge.

The remaining area is associated with the far-field temperature,  $T_f$ . It is calculated from the equation,

$$A_{3f} = A_{3d} = \pi(r_a + D_3)^2 - A_{1b} - A_{2a} \quad (46)$$

where  $D_3$  is the distance from the edge of the slab to the undisturbed ground in the far-field, or 12.5m [3].

The area through which heat is transferred between  $T_o$  and  $T_f$  is calculated from the Fourier equation for conduction through a hollow cylinder

$$Q = k \left( \frac{2\pi h}{\ln \frac{r_o}{r_i}} \right) \Delta T. \quad (47)$$

By the convention of the matrix definition, all equations are cast in the general form

$$Q_{ij} = \left( \frac{k_{ij} A_{ij}}{L_{ij}} \right) (T_i - T_j). \quad (48)$$

Therefore,

$$Q_{ef} = \frac{k_{ef} A_{ef}}{L_{ef}} (T_o - T_f) \quad (49)$$

so that

$$\frac{2\pi h}{\ln \frac{r_o}{r_i}} = \frac{2\pi L_{2o}}{\ln \frac{L_{bo} + L_{of}}{L_{bo}}} = \frac{A_{of}}{L_{of}} \quad (50)$$

and,

$$A_{of} = \frac{2\pi L_{2o} L_{of}}{\ln \frac{L_{bo} + L_{of}}{L_{bo}}} = \frac{2\pi (D_1)(D_3)}{\ln \frac{r_p + D_3}{r_p}}. \quad (51)$$

Similarly,

$$A_{23} = \frac{2\pi L_{2d} L_{23}}{\ln \frac{L_{bo} + L_{23}}{L_{12}}} = \frac{2\pi (D_2)(D_3)}{\ln \frac{r_p + D_3}{r_p}}. \quad (52)$$

It is postulated that the slab is isothermal to within  $d_1$  of the slab edge. It is therefore estimated that the area through which heat is transferred between  $T_b$  and  $T_o$  can also be calculated correspondingly:

$$A_{bo} = \frac{2\pi L_{1b}(d_1)}{\ln \frac{L_{bo}}{L_{bo} - d_1}} = \frac{2\pi (D_1)(d_1)}{\ln \frac{r_p}{r_p - d_1}}. \quad (53)$$

Again,  $A_{12}$  is calculated in a similar fashion:

$$A_{12} = \frac{2\pi L_{1d}(d_1)}{\ln \frac{L_{12}}{L_{12} - d_1}} = \frac{2\pi (D_2)(d_1)}{\ln \frac{r_p}{r_p - d_1}}. \quad (54)$$

The volumes associated with temperatures  $T_1$ ,  $T_2$ , and  $T_3$  are calculated by

$$V_1 = A_{1b} h_1 \quad (55)$$

$$V_2 = A_{2e} h_2$$

and

$$V_3 = A_{3f} h_3$$

$D_1$ ,  $D_2$ , and  $D_3$  are defined by temperature profiles of the undisturbed ground and do not change with slab size or shape. Referencing Section 3.3 and Figure 2,  $D_1$  is the distance between the inflection point and the diurnal penetration depth or,

$$D_1 = 4.0m - 0.5m = 3.5m. \quad (56)$$

$D_2$  is the distance between the undisturbed deep ground and the inflection point or,

$$D_2 = 15m - 4m = 11m \quad (57)$$

and  $D_3$  is the distance from the edge of the slab to undisturbed ground temperature in the vertical plane,

$$D_3 = 12.5m. \quad (58)$$

$h_1$ ,  $h_2$ , and  $h_3$  are assumed to be equal to each other and equal to half of the depth of the entire system:

$$h_1 = h_2 = h_3 = 14.5/2 = 7.25m. \quad (59)$$

The results of Bahnfleth [3] show that for rectangular slabs, surface temperature is nearly constant to within 1.0m of the edge regardless of slab size or aspect ratio. Based on these data  $d_1$  is assigned the value of 1.0m.

In the edge effect region, the direction of heat flux changes dramatically over the year. Temperature profiles developed by Bahnfleth [3], and Kusuda [5] show that in the region between the slab edge and roughly 3m outside the building edge, the direction of heat flux varies dramatically over the annual cycle. It is desirable that this region be distinguished from the regions where the heat flux patterns are more consistent over the annual cycle. Therefore, this region is characterized as the edge region and its area (in the plane of the ground surface),  $A_{2e}$ , is encircled by a boundary approximately 3.0m beyond the edge of the slab. Therefore,  $d_2$  is assigned the value of 3.0m.

For the test system,  $L$  becomes

$$L = \begin{pmatrix} 0 & 7.64 & 0 & 3.5 & 0 & 11 & 0 \\ 7.64 & 0 & 12.5 & 0 & 0 & 11 & 3.5 \\ 0 & 12.5 & 0 & 0 & 3.5 & 11 & 0 \\ 3.5 & 0 & 0 & 0 & 0 & 0 & 7.64 \\ 0 & 0 & 3.5 & 0 & 0 & 0 & 12.5 \\ 11 & 11 & 11 & 0 & 0 & 0 & 0 \\ 0 & 3.5 & 0 & 7.64 & 12.5 & 0 & 0 \end{pmatrix} \quad (60)$$

Substituting  $L_U$ ,  $r_p$ ,  $r_a$ ,  $d_1$  and  $d_2$  into the area equations and introducing the values into the matrix  $A$  gives

$$A = \begin{pmatrix} 0 & 492.6 & 0 & 104.6 & 0 & 104.6 & 0 \\ 492.6 & 0 & 891.2 & 0 & 0 & 195.3 & 195.3 \\ 0 & 891.2 & 0 & 0 & 866.7 & 866.7 & 0 \\ 104.6 & 0 & 0 & 0 & 0 & 0 & 156.7 \\ 0 & 0 & 866.7 & 0 & 0 & 0 & 283.6 \\ 104.6 & 195.3 & 866.7 & 0 & 0 & 0 & 0 \\ 0 & 195.3 & 0 & 156.7 & 283.6 & 0 & 0 \end{pmatrix} \quad (61)$$

The volume vector then becomes

$$V = \begin{pmatrix} 758 \\ 1416 \\ 6284 \end{pmatrix} m^3 \quad (62)$$

#### 4.4.1 MULTIPLE-INPUT TRANSFER FUNCTION COEFFICIENTS

Program GTF [see Appendix C] calculates the multiple-input ground transfer function (GTF) coefficients and scalar constants from the model structure and geometry and soil properties using the method of Seem. The GTF coefficients and scalar constants calculated for the test system with the geometric network parameters are:

$$S_0 = \begin{pmatrix} 4.3519192373e+006 & 3.9049689583e-003 & 9.7034921495e+002 & 1.7727765309e+006 \\ 3.9055744470e-003 & -2.3330414785e+007 & 8.0401375450e+009 & 1.9601062778e+006 \\ 9.7034921516e+002 & 8.0401375444e+003 & -9.1597479408e+006 & 1.8115962474e+003 \\ 1.7727765309e+006 & 1.9601062778e+006 & 1.8115962471e+003 & -8.5480206671e+006 \end{pmatrix} \quad (63)$$

$$S_1 = \begin{pmatrix} 1.2971329802e+007 & 4.2782186309e-002 & 9.5420141644e+002 & -5.2814397560e+006 \\ 4.2780380377e-002 & 6.9556564823e+007 & -7.9063398134e+003 & -5.8395307500e+006 \\ 9.5420141708e+002 & -7.9063398117e+003 & 2.7295669802e+007 & -1.7814490693e+003 \\ 5.2814397560e+006 & 5.8395307500e+006 & -1.7814490682e+003 & 2.5477632842e+007 \end{pmatrix}$$

$$S_2 = \begin{pmatrix} 1.2887351382e+007 & 4.2601077706e-002 & -9.6828788233e+002 & 5.2447951733e+006 \\ 4.2602873134e-002 & 6.9123847927e+007 & -8.0230577225e+003 & 5.7990140632e+006 \\ -9.6828788170e+002 & -8.0230577242e+003 & -2.7113081293e+007 & -1.8077478356e+003 \\ 5.2447951733e+006 & 5.7990140632e+006 & -1.8077478367e+003 & -2.5312101370e+007 \end{pmatrix}$$

$$S_3 = \begin{pmatrix} 4.2679401162e+006 & 3.8572502888e-003 & 9.5226778703e+002 & -1.7361314679e+006 \\ 3.8566553037e+003 & 2.2897696056e+007 & 7.8903181166e+003 & -1.9195889092e+006 \\ 9.5226778682e+002 & 7.8903181171e+003 & 8.9771580077e+006 & 1.7778390733e+003 \\ 1.7361314679e+006 & -1.9195889092e+006 & 1.7778390736e+003 & 8.3824877947e+006 \end{pmatrix}$$

$$e_1 = -2.97921 \quad (64)$$

$$e_2 = 2.95854$$

$$e_3 = -0.979329.$$

#### 4.4.2 INITIAL HEAT FLUX CALCULATIONS USING MULTIPLE INPUT TRANSFER FUNCTIONS

Program QCALC (see Appendix C) uses the GTFs and the input temperatures with Equation (5) to calculate the daily average heat flux. The results are divided by the slab area in order to be compatible in units with the base case data. Figure 8 shows the flux plot of the GTF model vs the finite difference model. Figure 9 plots the daily average flux of the GTF model and its difference from the FDM. Although annual period of the flux curve appears nearly correct, its amplitude is much too small. Because the magnitude of the maximum flux is fairly accurate, it is likely that the primary cause of the error is the assumption of too much mass in the system. The network parameters were based on the assumption that the mass associated with the system is composed of three cylinders of equal depth with cross-sectional areas equal to the area through which heat is transferred vertically in their respective regions. The resulting volume vector (Equation (62)) heavily weights the system mass with the far-field undisturbed ground temperature. The result is that the mass of soil directly beneath the slab has the least effect. This is obviously incorrect. Various changes to the model were introduced to improve its behavior. These are discussed in Section 4.5.

Figure 8: Flux -- FDM and Run 1A

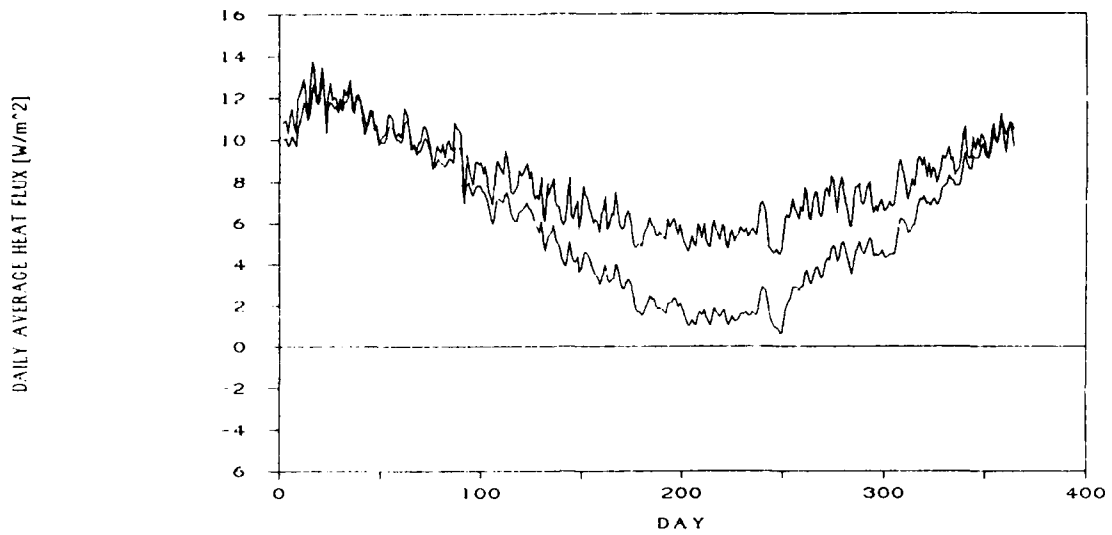
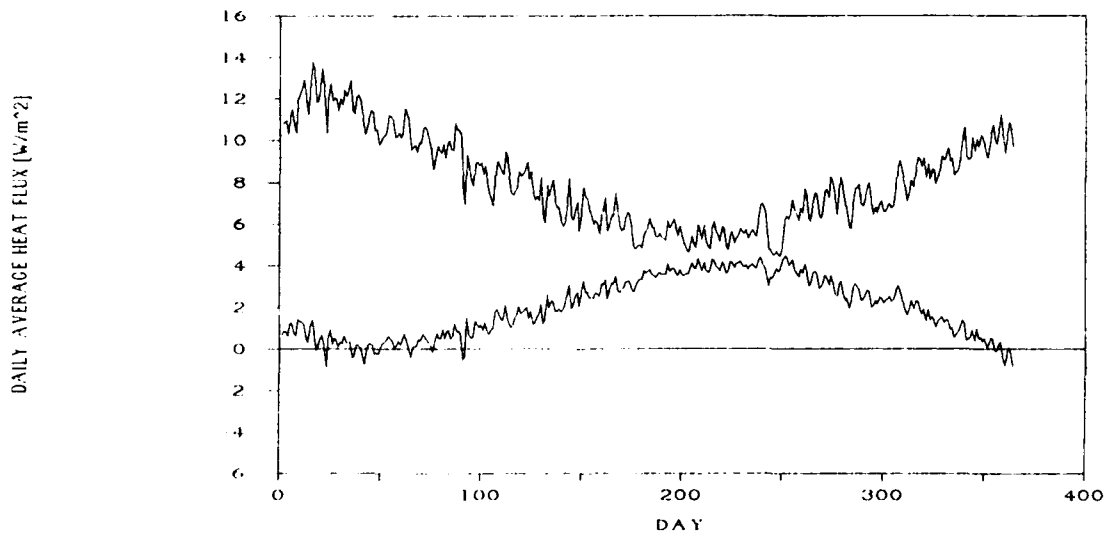


Figure 9: Flux and Difference -- Run 1A



## 4.5 PARAMETER REFINEMENT USING EMPIRICAL METHODS

### 4.5.1 MODEL BASED ON 12m X 12m SLAB

The effect of soil volume on the shape of the annual flux curve, although evident, is not easily described by geometric techniques. It may be possible to improve the accuracy of the model, particularly in cases where the daily average flux per unit area is small, by adjusting the model parameters based on improved fit to the base case data.

The original parameter set based on system geometry showed an excess of thermal mass in the system. Therefore, the volume vector was revised by reducing the depth of the cylinders of mass associated with  $V_2$  and  $V_3$  to 1m from 7.25m while leaving the mass associated with  $V_1$  intact. The volume vector then became

$$V = \begin{pmatrix} 758 \\ 195 \\ 867 \end{pmatrix} m^3. \quad (65)$$

The remaining parameters were held the same as the original run. Table 1 Run 1B presents the parameter set.

Program GTF was rerun with this new set of parameters and the results are shown in Figures 10 and 11.

Table 1: Parameter Sets for Runs 1A - 1C

	RUN 1A	RUN 1B	RUN 1C
$AREA [m^2]$	144	144	144
PERIMETER [m]	48	48	48
A/P [m]	3.0	3.0	3.0
$A_{fe}$	157	157	157
$A_{12}$	493	493	493
$A_{be}$	284	284	284
$A_{23}$	891	891	891
$A_{1b} = A_{1d}$	105	105	105
$A_{2d} = A_{2e}$	195	195	195
$A_{3f} = A_{3d}$	867	867	867
$V_1$	758	758	758
$V_2$	1416	195	195
$V_3$	6284	867	87

Figure 10: Flux -- FDM and Run 1B

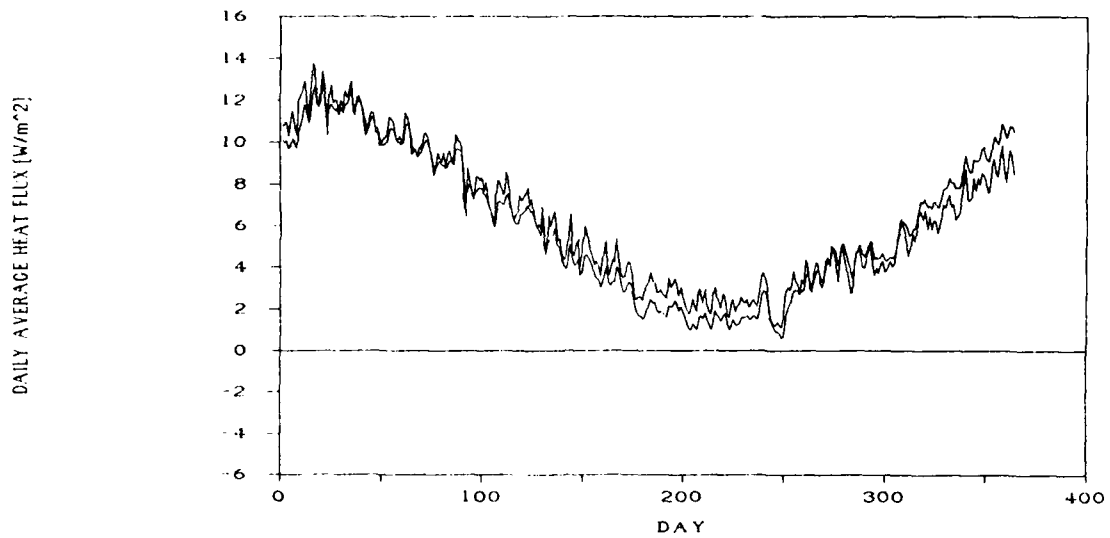


Figure 11: Flux and Difference -- Run 1B

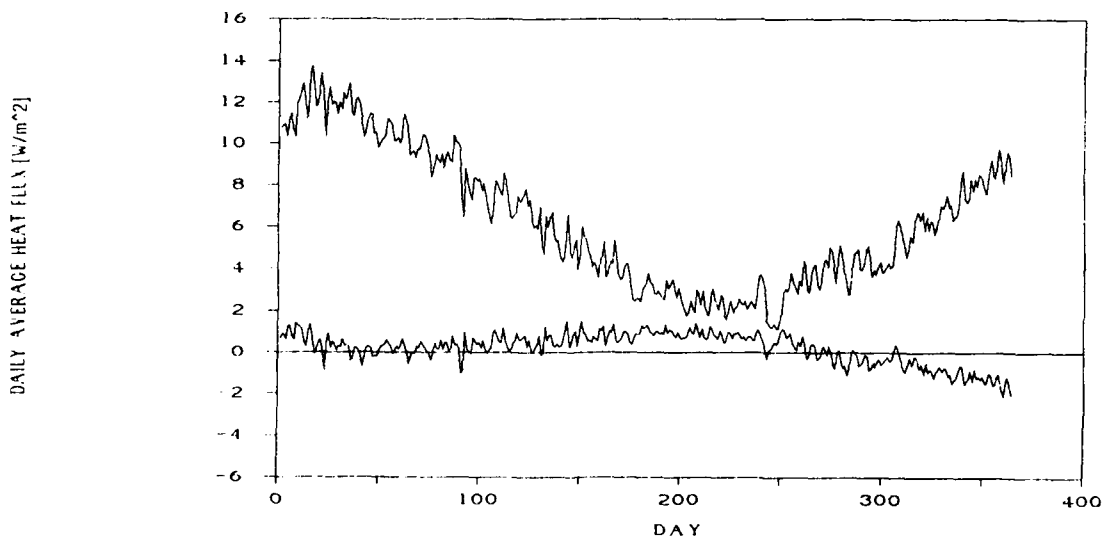


Figure 10 plots the daily average heat flux over the cycle for the base case FDM and the GTF Run 1B. Comparison with Figure 8 shows the substantial improvement in fit. Figure 11 shows the flux and the difference from the FDM results of Run 1B. Comparing Figure 9 with Figure 11 it can be seen that model 1B vastly reduces the model error in the summer-time data.

The new set of parameters leads to a better match of the base case data from which it can be inferred that the primary flaw in the original parameter set was indeed an excess of mass. Even though the revised set of parameters is substantially better than the original set, the figures indicate that more improvement is required. The annual amplitude of the curve is still slightly too small and the new set of parameters presents a new flaw in the model: the flux calculated for the end of the year becomes increasingly too small. This seems to indicate an imbalance in the mass distribution. The first step towards resolving this situation was to reduce the mass associated with the far-field region in an effort to both reduce the total mass of the system and place more emphasis on the mass immediately beneath the slab. The depth of the cylinder of mass associated with the far-field ( $h_3$ ) was reduced from 1m to 0.1 m. resulting in the new volume vector

$$V = \begin{pmatrix} 758 \\ 195 \\ 87 \end{pmatrix} m^3. \quad (66)$$

Once again, the remaining network parameters were held the same as the original run (see Table 1 Run 1C).

The new GTFs and scalar constants were used to recalculate the daily average heat flux. The resulting flux and difference plots are given in Figures 12 and 13. On a plot of the daily average flux (Figure 12) Run 1C and the FDM are practically indistinguishable. Figure 13 presents the flux calculated in Run 1C and the difference between Run 1C and the FDM. Except for a few points early in the annual cycle when the flux is high, the difference between Run 1C and the FDM is less than  $1 \text{ W/m}^2$ .

The match between the FDM and Run 1C is significantly better than both Run 1a and Run 1b. Table 2 gives a numerical comparison of the three GTF models with the base case finite difference model. It can be seen that 90% of the data were within 15% of the FDM and the percent error in total energy consumption over the annual cycle is -1.0%.

Figure 12: Flux -- FDM and Run 1C

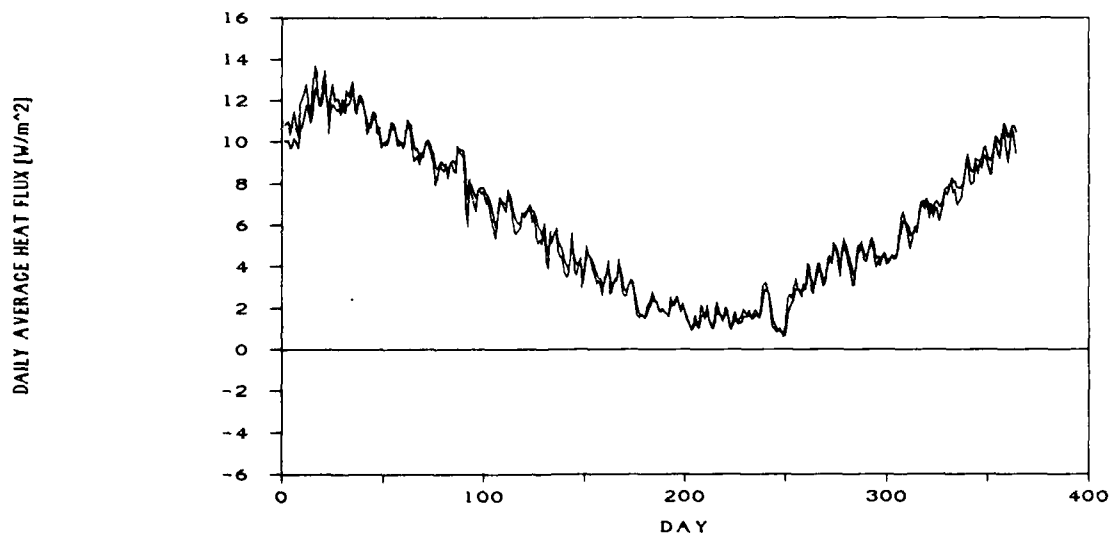


Figure 13: Flux and Difference Run 1C

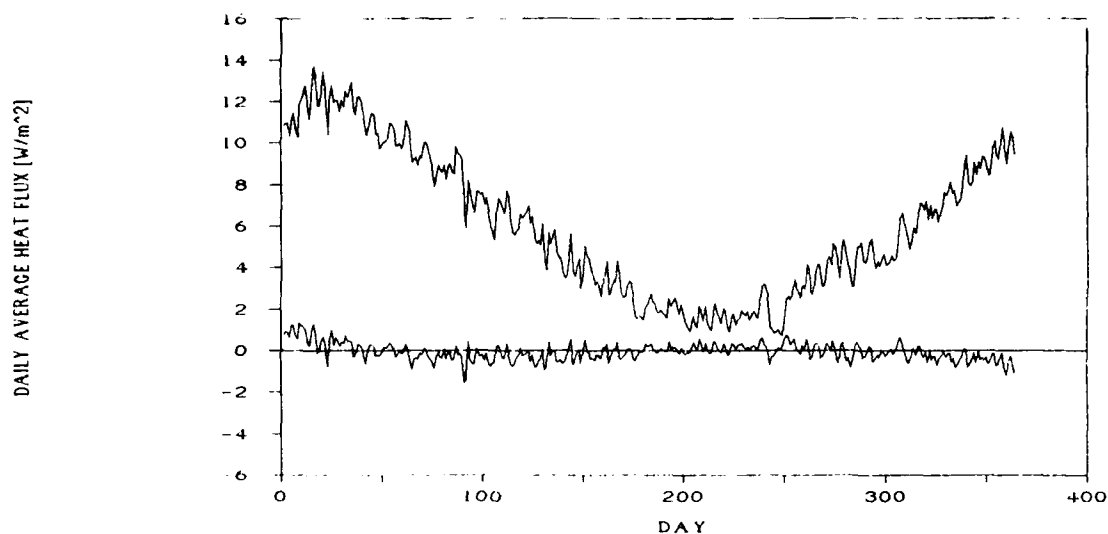


Table 2: Results of Runs 1A - 1C

MODEL	MEAN FLUX [W/m <sup>2</sup> ]	SUM OF SQUARED DIFF	% OF DATA WITHIN 15% OF FDM [%]	TOTAL ANNUAL ENERGY CONSUMP	% ERROR IN TOTAL ENERGY CONSUMP [%]	TOTAL ANNUAL DIFF IN ENERGY CONSUMP
FDM	6.10	-----	-----	7716.9	-----	-----
RUN 1A	8.10	2149.2	37	10194.4	24.3	+2477.5
RUN 1B	6.35	214.2	64	7984.4	3.4	+267.5
RUN 1C	6.07	69.9	90	7641.4	-1.0	-75.5

#### 4.5.2 MODEL CORRECTIONS BASED ON 45m X 45m SLAB

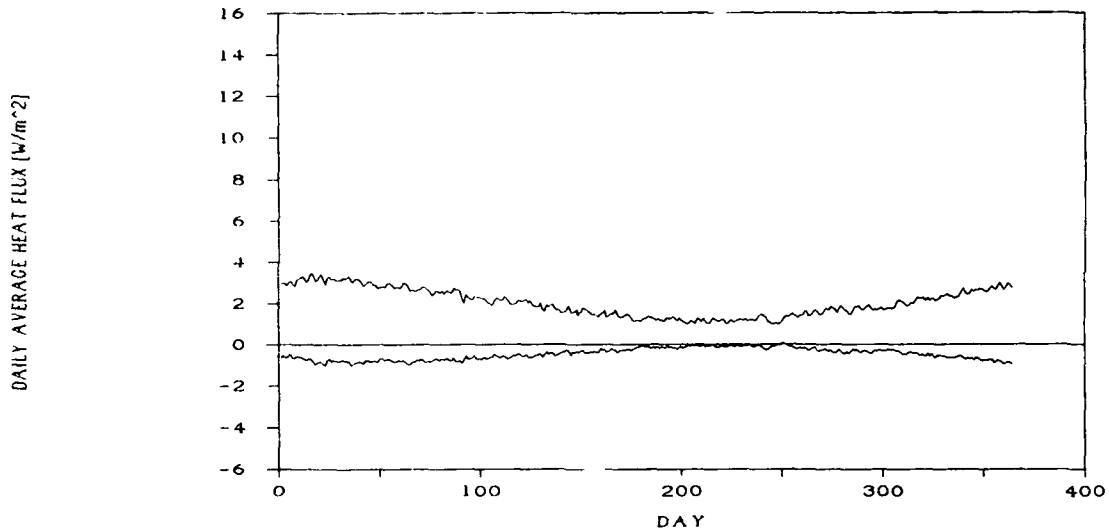
Using the same parameter equations as Run 1C, changing only  $r_p$  and  $r_a$ , the GTFs and scalar constants were recalculated for the larger (45m x 45m) slab. The resulting parameter set is shown in the column labeled Run 2A in Table 3.

Table 3: Parameter Sets for Runs 2A - 2D

	RUN 2A	RUN 2B	RUN 2C	RUN 2D
AREA [ $m^2$ ]	2025	2025	2025	2025
PERIMETER [m]	180	180	180	180
A/P [m]	11.25	11.25	11.25	11.25
$A_{fe}$	619	619	1113	1113
$A_{12}$	1945	1945	1945	1945
$A_{be}$	759	759	1113	1113
$A_{23}$	2386	2386	3499	3499
$A_{1b} = A_{1d}$	1869	1869	1869	1869
$A_{2d} = A_{2e}$	663	2349	663	879
$A_{3f} = A_{3d}$	1978	293	1978	1762
$V_1$	13548	13548	13548	13548
$V_2$	663	2349	663	879
$V_3$	198	29	198	176

Figure 14 compares the output for the 45m x 45m slab of the GTF model and the FDM base case.

Figure 14: Flux and Difference -- Run 2A



There is a distinct droop of the GTF during the winter season, the time when the edge effect is strongest. During the summer season when the edge effect is small, the GTF model is quite accurate. This suggests that for larger slabs the method for calculating the parameter set does not account adequately for the edge effect. Returning to the original energy balance on the edge node

$$\frac{k_{be}A_{be}}{L_{be}}(T_e - T_b) + \frac{k_{2e}A_{2e}}{L_{2e}}(T_e - T_2) + \frac{k_{fe}A_{fe}}{L_{fe}}(T_e - T_f) = Q_e \quad (67)$$

and recalling that for this study  $T_e = T_b$ , we see that there are three likely causes for underprediction of edge loss. The first possibility is that  $A_{2e}$  is too small so that loss to the ground beneath the edge is underpredicted. An adjustment to  $A_{2e}$  should produce a generally linear change in the flux, although the seasonal change of  $T_2$  will modify

that effect to some extent. The second possibility is that the area  $A_{fe}$  is too small so that heat flux directly to the ground surface is insufficient. Thirdly, the temperature node  $T_2$  may be too high. This is most likely to result from a deficient  $A_{23}$  which would lead to a reduction in the heat transferred from the node beneath the slab edge (node 2) to the node at 4 meters depth in the far-field (node 3) thereby maintaining an inappropriately elevated  $T_2$ .

Two studies were performed in order to determine the most likely cause of the underprediction of edge loss in the larger slab. The first investigates the effects of increasing  $A_{2e}$ . The second explores the possibility of improving the model fit by increasing  $A_{23}$  and  $A_{fe}$ .

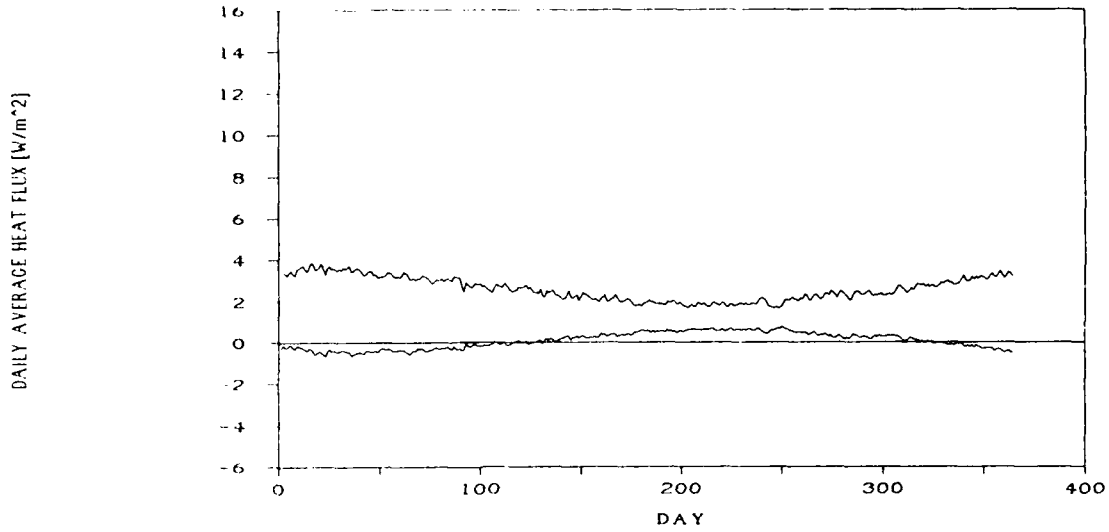
Inspection of the parameter sets shows that in parameter set 1 (used for the smaller slab) the area through which heat is transferred directly from the slab core to the earth ( $A_{1e}$ ) is nearly half the area through which heat is transferred directly from the slab edge to the earth ( $A_{2e}$ ). In parameter set 2, however, the trend is reversed so that  $A_{1e}$  is nearly three times  $A_{2e}$ . While it is anticipated that the effect of the core area would increase as the slab becomes larger, this dramatic change seems excessive, a notion which is reinforced by the apparent underprediction of the edge effect from parameter set 1. A possible source of error is the determination of the distance the edge effect extends beyond the slab edge ( $d_2$ ). It is interesting to note that this distance is equal to the characteristic length ( $\frac{A}{P}$ ) of the smaller slab. It is postulated, therefore, that  $d_2$  should be defined by the slab characteristic length rather than by a constant. A new set of parameters (see Run 2B in Table 3) is established based on this theory. The daily

average flux calculated by this new set of parameters and the difference from the FDM are shown in Figure 15. The curve shows a better fit of the data particularly during the winter season when the flux is highest. Examination of the difference between the FDM and GTF Run 2B, however, shows that the model still demonstrates a systematic seasonal error. Comparing Figure 14 and Figure 15, it can be seen that increasing  $A_2$  has produced a linear increase in the heat flux throughout the annual cycle. Nonetheless, the model is reasonably accurate over the annual cycle giving an error of 3.6% in total annual energy loss. Table 4 gives a numerical comparison of GTF models 2A and 2B with the base case FDM.

Table 4: Results of Runs 2A and 2B

MODEL	MEAN FLUX [W/m <sup>2</sup> ]	SUM OF SQUARED DIFF	% OF DATA WITHIN 15% OF FDM [%]	TOTAL ANNUAL ENERGY CONSUMP	% ERROR IN TOTAL ENERGY CONSUMP [%]	TOTAL ANNUAL DIFF IN ENERGY CONSUMP
FDM	2.50	-----	-----	44167.7	-----	-----
RUN 2A	2.03	106.9	33	35911.3	-18.7	-8256.4
RUN 2B	2.59	54.0	64	45762.0	+3.6	+1594.3

Figure 15: Flux and Difference -- Run 2B



$A_{23}$  and  $A_{fe}$  are geometrically similar (see eqns 51 and 52). The correction is made originally on  $A_{23}$  because the  $T_2$ - $A_{23}$ - $T_3$  system is more stable than the  $T_e$ - $A_{fe}$ - $T_f$  system. The correction is then applied to both  $A_{23}$  and  $A_{fe}$ . The determination of the corrected  $A_{23}$  is based on the assumption of a functional relationship between  $A_{23}$  and the slab characteristic length. Characteristic length is discussed in more detail in Section 6.  $A_{23}$  is calculated from the equation

$$A_{23} = 2\pi r_{equiv} L_{2d} \quad (68)$$

Assuming that  $A_{23} = 891 m^2$  is correct for the small slab

$$A_{23} = 891 = 2\pi r_{equiv} L_{2d} = 2\pi r_{equiv} (11) \quad (69)$$

so that

$$r_{equiv} = \frac{891}{2\pi(11)} = 13 \quad (70)$$

If  $r_{equiv}$  is assumed to be a simple function of characteristic length, a functional relationship can be postulated. Suppose

$$r_{equiv} = K * (\text{characteristic length}) \quad (71)$$

The characteristic length (A/P) of the small slab is 3.0m. So, from Equations (70) and (71),

$$r_{equiv} = 13 = K * 3.0 \quad (72)$$

so that K is approximately equal to 4.5. Then, using Equation (71), Equation (68) becomes

$$A_{23} = 2\pi L_{2d}(4.5)(\text{characteristic length}). \quad (73)$$

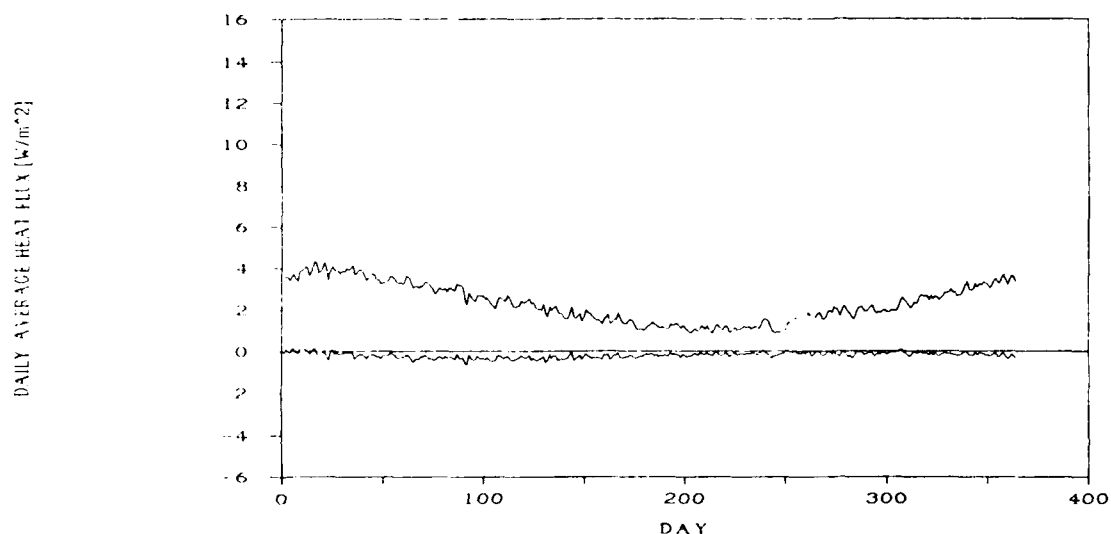
Similarly,

$$A_{ef} = 2\pi L_{2e}(4.5)(\text{characteristic length}). \quad (74)$$

The parameter set for Run 2C is given in Table 3. GTFs and daily average heat fluxes are recalculated with the new  $A_{23}$  and  $A_{ef}$ . The numerical comparison of Run 2C to the FDM and Runs 2A and 2B is tabulated in Table 5. Run 2C shows a significantly improved fit to the FDM data as evidenced by the substantial decrease in the sum of squared difference and the percentage of the GTF data within 15% of the FDM

data. Unfortunately, this improvement in fit was accompanied by an increase in the total error over the annual cycle. Examination of the plot of the difference between the results of RUN 2C and the base case FDM (Figure 16) shows that the wintertime droop has been corrected, but there is still a linear underprediction of slab loss.

Figure 16: Flux and Difference -- Run 2C



It was demonstrated by Run 2B that such an error might be corrected by an adjustment of  $A_{2e}$ , however, an adjustment of the magnitude of 2B is unnecessary. Once again, a possible source of error is the determination of the distance that the edge effect extends beyond the slab edge ( $d_2$ ). If  $d_2$  is assumed to be a function of slab characteristic length of the form

$$d_2 = c + m(\text{characteristic length}) \quad (75)$$

then  $c$  and  $m$  can be chosen so that  $d_2$  varies with slab geometry. Based on the results of the small slab,  $c$  is probably less than 3.0 and  $m$  less than 1.0. If  $c$  is assumed to be 2.5m then  $m$  can be calculated from the model of the 12m x 12m slab.

$$3.0 = 2.5 + m(3.0) \quad (76)$$

which gives

$$m = \frac{3.0 - 2.5}{3.0} \quad (77)$$

which is approximately equal to 0.15. When the equation

$$d_2 = 2.5 + 0.15(\text{characteristic length}) \quad (78)$$

is applied the new values of  $d_2$  become:  
for the smaller slab

$$d_2 = 2.95 \quad (79)$$

and for the larger slab

$$d_2 = 4.19 \quad (80)$$

The parameter set is recalculated and given in Table 3, Run 1D. When this change is made in the calculations for the larger slab the result is a significantly improved fit to the FDM base case. The flux and difference curves are shown in Figure 17. As expected, the difference curve has shifted linearly, moving nearer to the zero difference line. The

numerical comparisons are given in Table 5. The quality of the fit (as measured by the sum of squared difference and percentage of data within 15% of the FDM) is improved as is the total energy consumption.

Figure 17: Flux and Difference -- Run 2D

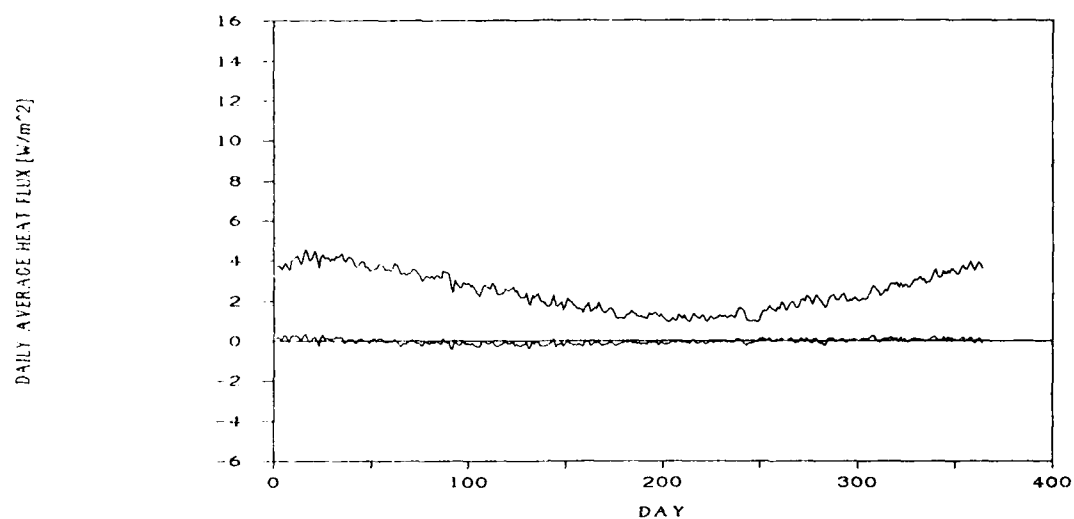


Table 5: Results of Runs 2A - 2D

MODEL	MEAN FLUX [W/m <sup>2</sup> ]	SUM OF SQUARED DIFF	% OF DATA WITHIN 15% OF FDM [%]	TOTAL ANNUAL ENERGY CONSUMP	% ERROR IN TOTAL ENERGY CONSUMP [%]	TOTAL ANNUAL DIFF IN ENERGY CONSUMP
FDM	2.50	-----	-----	44167.7	-----	-----
RUN 2A	2.03	106.9	33	35911.3	-18.7	-8256.4
RUN 2B	2.59	54.0	64	45762.0	+3.6	+1594.3
RUN 2C	2.31	19.9	83	40780.2	-7.7	-3387.5
RUN 2D	2.42	8.1	97	42872.2	-2.9	-1295.5

#### 4.5.3 CORRECTED MODEL APPLIED TO 12m X 12m SLAB

Because the modifications have changed the functional relationships which effect the original parameter set, it is necessary to recalculate the parameter set for the smaller slab and recalculate the daily average fluxes as Run 1D. A comparison of the parameter sets of Runs 1A-1D is given in Table 6 and the results in Table 7. The quality of the fit as determined by the sum of squared difference is slightly degraded by the changes made for Run 1D. Nonetheless, the improvement of the fit of the model to the data for the larger slab more than justifies the change.

Table 6: Parameter Sets for Runs 1A - 1D

	RUN 1A	RUN 1B	RUN 1C	RUN 1D
AREA [ $m^2$ ]	144	144	144	144
PERIMETER [m]	48	48	48	48
A/P [m]	3.0	3.0	3.0	3.0
$A_{fe}$	157	157	297	297
$A_{12}$	493	493	493	493
$A_{be}$	284	284	284	297
$A_{23}$	891	891	891	933
$A_{1b} = A_{1d}$	105	105	105	105
$A_{2d} = A_{2e}$	195	195	195	192
$A_{3f} = A_{3d}$	867	867	867	870
$V_1$	758	758	758	758
$V_2$	1416	195	195	192
$V_3$	6284	867	87	87

Table 7 Results of Runs 1A - 1D

MODEL	MEAN FLUX [W/m <sup>2</sup> ]	SUM OF SQUARED DIFF	% OF DATA WITHIN 15% OF FDM [%]	TOTAL ANNUAL ENERGY CONSUMP	% ERROR IN TOTAL ENERGY CONSUMP [%]	TOTAL ANNUAL DIFF IN ENERGY CONSUMP
FDM	6.13	-----	-----	7716.9	-----	-----
RUN 1A	8.10	2149.2	37	10194.4	24.3	+2477.5
RUN 1B	6.35	214.2	64	7984.4	3.4	+267.5
RUN 1C	6.07	69.9	90	7641.4	-1.0	-75.5
RUN 1D	6.19	82.0	89	7786.6	+0.9	+69.1

## 5 FINAL DEFINITION AND TESTING

### 5.1 FINAL DEFINITION

The model used for Runs 1D and 2D gives excellent results for both the 12m x 12m square slab and the 45m x 45m square slab. The parameter sets generated for both these runs were constructed from the same series of equations developed using both geometric and empirical methods. The equations are repeated here in their final forms.

$$D_1 = 4.0m - 0.5m = 3.5m. \quad (81)$$

$$D_2 = 15m - 4m = 11m \quad (82)$$

$$D_3 = 12.5m \quad (83)$$

$$d_1 = 1.0m \quad (84)$$

$$d_2 = 2.5 + 0.15(\text{characteristic length}) \quad (85)$$

$$h_1 = \frac{D_1 + D_2}{2} = 7.25m. \quad (86)$$

$$h_2 = 1.0m \quad (87)$$

$$h_3 = 0.1m \quad (88)$$

$$L_{1b} = L_{2e} = L_{3f} = D_1 \quad (89)$$

$$L_{1d} = L_{2d} = L_{3d} = D_2 \quad (90)$$

$$L_{fe} = L_{23} = D_3. \quad (91)$$

$$r_p = \frac{P}{2\pi}. \quad (92)$$

$$r_c = \sqrt{\frac{A}{\pi}}. \quad (93)$$

$$A_{bo} = \frac{2\pi(D_1)(d_1)}{\ln \frac{r_p}{r_p - d_1}} \quad (94)$$

$$A_{ef} = 2\pi L_{2e}(4.5)(\text{characteristic length}) \quad (95)$$

$$A_{12} = \frac{2\pi(D_2)(d_1)}{\ln \frac{r_p}{r_p - d_1}} \quad (96)$$

$$A_{23} = 2\pi L_{2d}(4.5)(\text{characteristic length}) \quad (97)$$

$$A_{1b} = A_{1d} = \pi(r_a - d_1)^2 \quad (98)$$

$$A_{2e} = A_{2d} = \pi(r_a + d_2)^2 - A_{1b} \quad (99)$$

$$A_{3f} = A_{3d} = \pi(r_a + D_3)^2 - A_{1b} - A_{2e} \quad (100)$$

$$V_1 = A_{1b}h_1 \quad (101)$$

$$V_2 = A_{2e}h_2 \quad (102)$$

$$V_3 = A_{3f}h_3 \quad (103)$$

These equations are used to construct the matrices

$$A = \begin{pmatrix} 0 & A_{12} & 0 & A_{1b} & 0 & A_{1d} & 0 \\ A_{12} & 0 & A_{23} & 0 & 0 & A_{2d} & A_{2e} \\ 0 & A_{23} & 0 & 0 & A_{3f} & A_{3d} & 0 \\ A_{1b} & 0 & 0 & 0 & 0 & 0 & A_{be} \\ 0 & 0 & A_{3f} & 0 & 0 & 0 & A_{fe} \\ A_{1d} & A_{2d} & A_{3d} & 0 & 0 & 0 & 0 \\ 0 & A_{2e} & 0 & A_{be} & A_{fe} & 0 & 0 \end{pmatrix} \quad (104)$$

$$L = \begin{pmatrix} 0 & L_{12} & 0 & L_{1b} & 0 & L_{1d} & 0 \\ L_{12} & 0 & L_{23} & 0 & 0 & L_{2d} & L_{2e} \\ 0 & L_{23} & 0 & 0 & L_{3f} & L_{3d} & 0 \\ L_{1b} & 0 & 0 & 0 & 0 & 0 & L_{be} \\ 0 & 0 & L_{3f} & 0 & 0 & 0 & L_{fe} \\ L_{1d} & L_{2d} & L_{3d} & 0 & 0 & 0 & 0 \\ 0 & L_{2e} & 0 & L_{be} & L_{fe} & 0 & 0 \end{pmatrix}. \quad (105)$$

$$V = \begin{pmatrix} V_1 \\ V_2 \\ V_3 \end{pmatrix} \quad (106)$$

The geometry matrices **A**, **L** and **V**, along with the soil property matrices  $k$ ,  $\rho$ , and  $c_p$  are used to calculate the matrices

$$G = \begin{pmatrix} 0 & G_{12} & 0 & G_{1b} & 0 & G_{1d} & 0 \\ G_{12} & 0 & G_{23} & 0 & 0 & G_{2d} & G_{2e} \\ 0 & G_{23} & 0 & 0 & G_{3f} & G_{3d} & 0 \\ G_{1b} & 0 & 0 & 0 & 0 & 0 & G_{be} \\ 0 & 0 & G_{3f} & 0 & 0 & 0 & G_{fe} \\ G_{1d} & G_{2d} & G_{3d} & 0 & 0 & 0 & 0 \\ 0 & G_{2e} & 0 & G_{be} & G_{fe} & 0 & 0 \end{pmatrix}. \quad (107)$$

$$C = \begin{pmatrix} C_1 \\ C_2 \\ C_3 \end{pmatrix} \quad (108)$$

by the equations

$$G_{ij} = \frac{k_{ij} A_{ij}}{l_{ij}} \quad (109)$$

and

$$C_i = \rho_i C_{pi} V_i. \quad (110)$$

These, in turn, are used to generate the coefficient matrices

$$A = \begin{pmatrix} \frac{-G_{1b} - G_{12} - G_{1d}}{C_1} & \frac{G_{12}}{C_1} & 0 \\ \frac{G_{12}}{C_2} & \frac{-G_{2a} - G_{12} - G_{23} - G_{2d}}{C_2} & \frac{G_{23}}{C_2} \\ 0 & \frac{G_{23}}{C_3} & \frac{-G_{3f} - G_{23} - G_{3d}}{C_3} \end{pmatrix} \quad (111)$$

$$B = \begin{pmatrix} \frac{G_{1b}}{C_1} & 0 & \frac{G_{1d}}{C_1} & 0 \\ 0 & 0 & \frac{G_{2d}}{C_2} & \frac{G_{2e}}{C_2} \\ 0 & \frac{G_{3f}}{C_3} & \frac{G_{3d}}{C_3} & 0 \end{pmatrix} \quad (112)$$

$$C = \begin{pmatrix} G_{1b} & 0 & 0 \\ 0 & 0 & G_{3f} \\ G_{1d} & G_{2d} & G_{3d} \\ 0 & G_{2e} & 0 \end{pmatrix} \quad (113)$$

$$D = \begin{pmatrix} -G_{1b} - G_{be} & 0 & 0 & G_{be} \\ 0 & -G_{3f} - G_{ef} & 0 & G_{ef} \\ 0 & 0 & -G_{1d} - G_{2d} - G_{3d} & 0 \\ G_{be} & G_{ef} & 0 & -G_{be} - G_{ef} - G_{2e} \end{pmatrix} \quad (114)$$

which are used with Seem's method to calculate the final multiple input GTFs and scalar constants which for the 12m x 12m slab are:

$$S_a = \begin{pmatrix} 2.0458127189e+000 & -2.1841677414e+007 & 5.3595180348e+005 & 2.0549408110e+006 \\ 9.8111895231e+002 & 5.3595180348e+005 & -8.9880223736e+006 & 1.3598085940e+004 \\ 1.7728083144e+006 & 2.0549408110e+006 & 1.3598085940e+004 & -8.5302667268e+006 \end{pmatrix} \quad (115)$$

$$S_b = \begin{pmatrix} 1.1698513689e+007 & 2.1005076402e+001 & -6.3178341430e+002 & -4.7628513469e+006 \\ 2.1005076393e+001 & 6.1491664962e+007 & -5.4126819711e+005 & -5.5054928856e+006 \\ 6.3178341430e+002 & -5.4126819711e+005 & 2.4444345580e+007 & -7.2500445257e+003 \\ -4.7628513469e+006 & -5.5054928856e+006 & -7.2500445257e+003 & 2.2994803858e+007 \end{pmatrix} \quad (116)$$

$$S_c = \begin{pmatrix} -1.0412722758e+007 & 1.9581095225e+001 & -9.6762874788e+002 & 4.2374081459e+006 \\ 1.9581095233e+001 & -5.7622418860e+007 & -4.4631067827e+005 & 4.8968796115e+006 \\ -9.6762874787e+002 & -4.4631067827e+005 & -2.2049931343e+007 & -1.4768777916e+004 \\ 4.2374081459e+006 & 4.8968796115e+006 & -1.4768777916e+004 & -2.0523358176e+007 \end{pmatrix} \quad (117)$$

$$S_d = \begin{pmatrix} 3.0658049564e+006 & 1.6560367478e+000 & 6.7715988886e+002 & -1.2471449406e+006 \\ 1.6560367454e+000 & 1.7971572628e+007 & 4.5211655346e+005 & -1.4460026224e+006 \\ 6.7715988886e+002 & 4.5211655346e+005 & 6.5929516101e+006 & 8.5289148747e+003 \\ -1.2471449406e+006 & -1.4460026224e+006 & 8.5289148747e+003 & 6.0581677786e+006 \end{pmatrix} \quad (118)$$

$$e_1 = -2.68674 \quad (119)$$

$$e_2 = 2.39032$$

$$e_3 = -0.703485.$$

## 5.2 VALIDATION

The final set of GTF coefficients and scalar constants calculated using the above equations are used to test the model for a variety of conditions including diverse climates, slab size and shape, and sensitivity to input data.

### 5.2.1 SIZE

The effect of slab size on the accuracy of the model has been described in Section 4.5. In summary, the model is quite accurate for relatively small ( $144 \text{ m}^2$ ) to relatively large ( $2025 \text{ m}^2$ ) square slabs giving an error in total annual energy consumption of less than 3% in both cases. The model is slightly more accurate overall for the larger slab based on the percentage of the data within 15% of the FDM: 97% for the larger slab vs. 89% for the smaller slab.

### 5.2.2 CLIMATE

The final GTF coefficients and scalar constants were used with environmental data for Medford OR, Philadelphia PA, and Phoenix AZ. Plots of the flux and difference for all four locations are given in Figures 18,19,20 and 21. Table 8 gives numerical data regarding the accuracy of the models. For Minneapolis, Medford, and Philadelphia, the difference between the GTF model and the FDM is very nearly zero. In all cases the difference is less than  $1 \text{ W/m}^2$  except for a few days at the beginning of the annual cycle. In Phoenix where the annual mean flux is approximately  $1.5 \text{ W/m}^2$ , an error of less than  $1 \text{ W/m}^2$  can create a significant error when the actual value of the error is quite small.

Figure 18: Flux and Difference -- Minneapolis MN

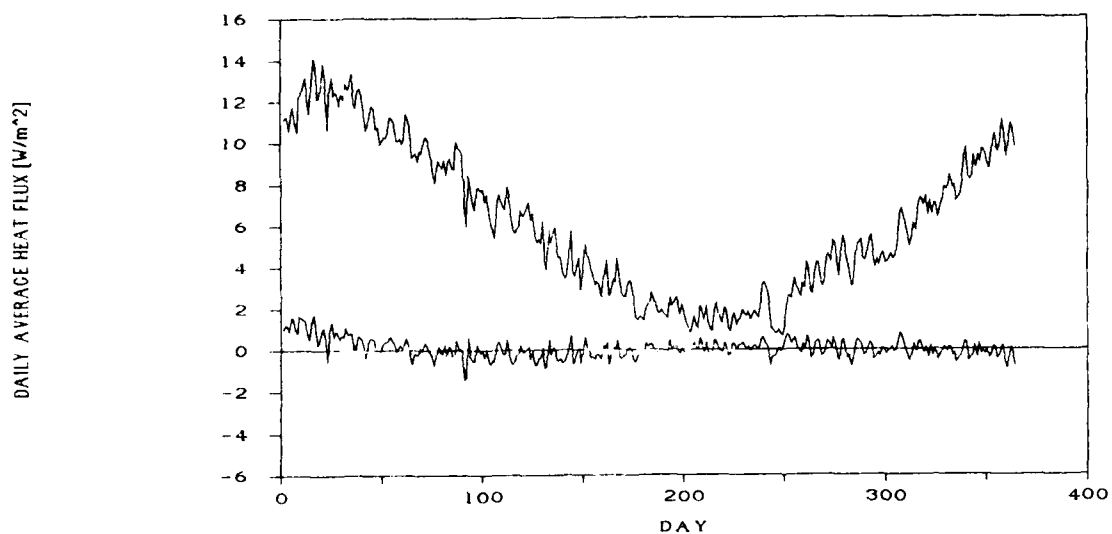


Figure 19: Flux and Difference -- Medford OR

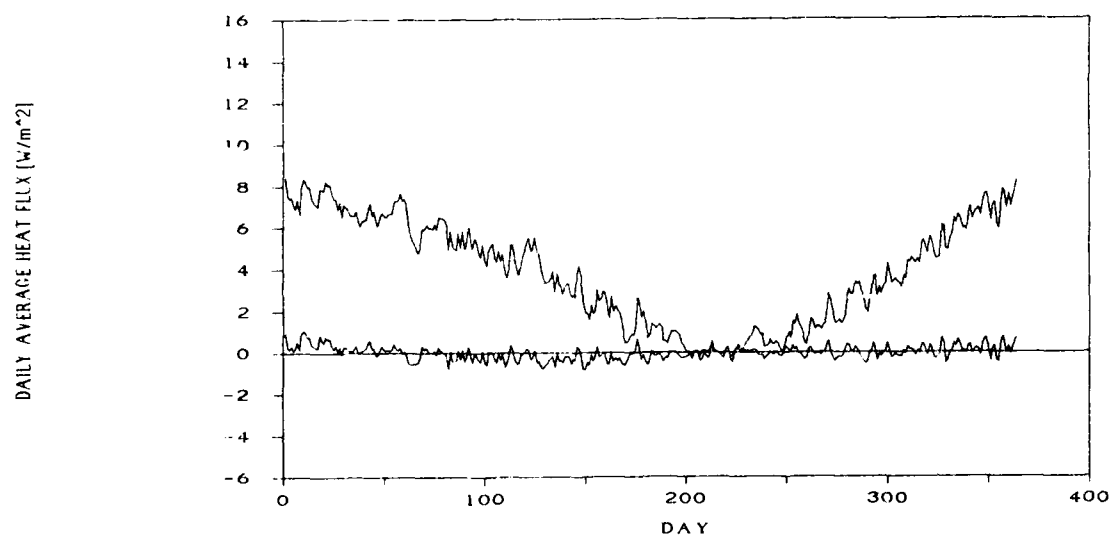


Figure 20: Flux and Difference -- Philadelphia PA

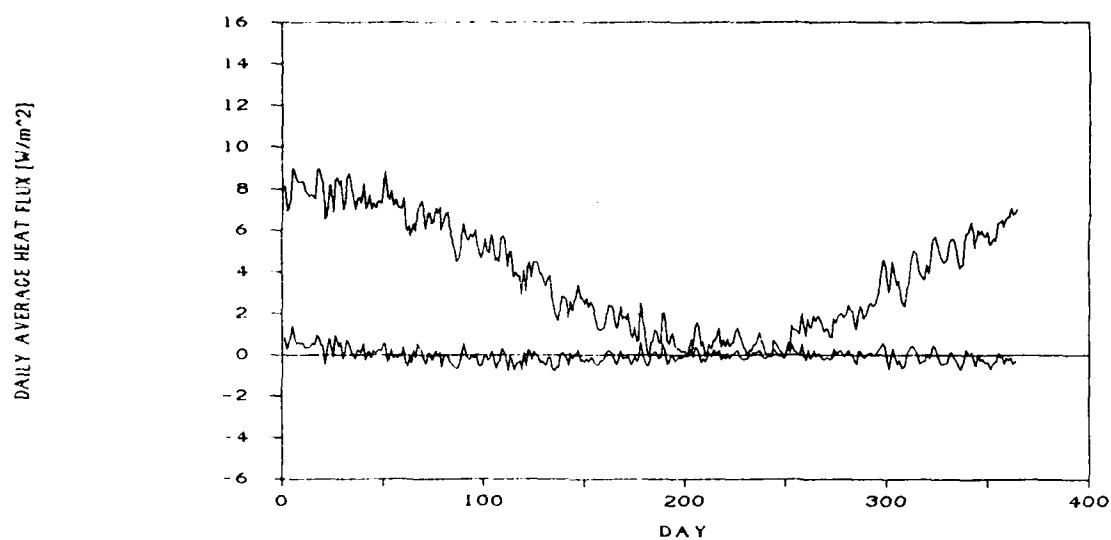


Figure 21: Flux and Difference -- Phoenix AZ

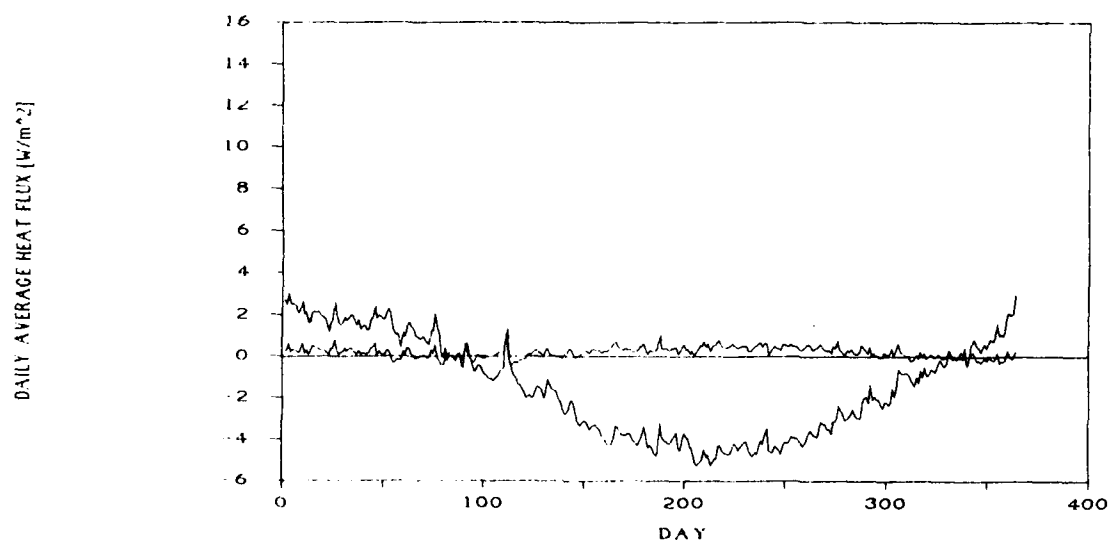


Table 8: Results of GTF Models for Various Locations

MODEL	LOCATION	MEAN FLUX [W/m <sup>2</sup> ]	% OF DATA WITHIN 15% OF FDM [%]	TOTAL ANNUAL ENERGY CONSUMP [kWhr]	% ERROR IN TOTAL ENERGY CONSUMP [%]	TOTAL ANNUAL DIFF IN ENERGY CONSUMP [kWhr]
FDM	Minneapolis	6.10	-----	7716.9	-----	-----
GTF	Minneapolis	6.19	89	7786.6	+0.9	+69.7
FDM	Medford	3.87	-----	4867.1	-----	-----
GTF	Medford	3.86	78	4856.6	-0.2	-10.5
FDM	Philadelphia	3.89	-----	4893.7	-----	-----
GTF	Philadelphia	3.87	78	4863.0	-0.6	-30.7
FDM	Phoenix	-1.66	-----	-2082.9	-----	-----
GTF	Phoenix	-1.46	72	-1832.7	-12.0	+250.2

### 5.2.3 SHAPE

This model was developed assuming a square slab and uses the circular isotherms which evolve as the result of that geometry. Although it was not expected that this model would adequately model non-square slabs, the extent of the inaccuracy was unknown. Therefore, parameter sets were constructed based on the slab perimeters and areas and using the above equations. These parameter sets were used to calculate GTF coefficient matrices and scalar constants, and

from them, daily average heat fluxes. The results are shown in Figures 22 and 23. Numerical comparison of these results to the FDM results for the non-square slabs is given in Table 9.

As was anticipated, the model does not give good results for non-square slabs. The form of the errors indicates an inaccuracy in the calculation of the edge effect. In the summer when the area effect dominates, the difference between the FDM and the GTF model is nearly zero. However, as the ground surface temperature drops and the edge effect becomes more important, the difference between the FDM and the GTF model shows an increasing underprediction of the slab heat loss.

Figure 22: Flux and Difference -- 6 x 24 Rectangle

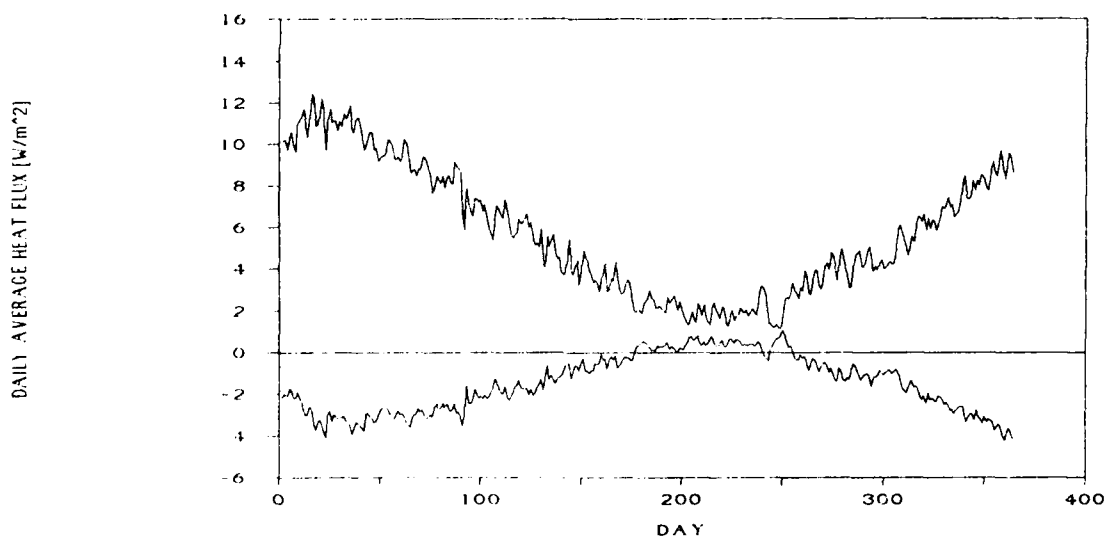


Figure 23: Flux and Difference -- 18 x 112 Rectangle

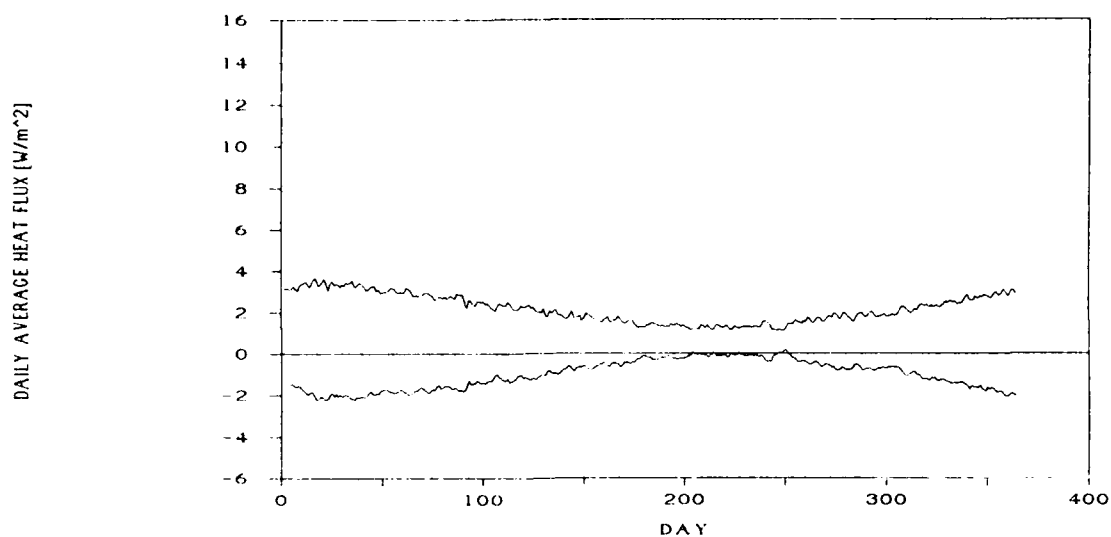


Table 9: Results of GTF Model for Non-square Slabs

MODEL	SLAB SIZE [m <sup>2</sup> ]	MEAN FLUX [W/m <sup>2</sup> ]	% OF DATA WITHIN 15% OF FDM [%]	TOTAL ANNUAL ENERGY CONSUMP [kWhr]	% ERROR IN TOTAL ENERGY CONSUMP [%]	TOTAL ANNUAL DIFF IN ENERGY CONSUMP [kWhr]
FDM	6 x 24	7.30	-----	9180.2	-----	-----
GTF	6 x 24	5.81	19	7305.2	-25.7	-1875.0
FDM	18 x 112	3.19	-----	56405.2	-----	-----
GTF	18 x 112	2.18	19	38530.3	-31.7	-17874.9

#### 5.2.4 SENSITIVITY TO INPUTS

It is important to understand the effect of the accuracy of the input data on the results of the model particularly if the required data are not available and approximations must be made. The most probable approximations are:

- (1) substituting daily average outdoor dry bulb temperature for daily average ground surface temperature ( $T_g$ )
- (2) substituting annual average outdoor dry bulb temperature for annual average ground surface temperature ( $T_d$ )
- (3) substituting constant indoor air temperature for daily average floor surface temperature ( $T_b$ ) and daily average floor edge temperature ( $T_e$ ).

These approximations will be tested for the 12m x 12m slab with the four climatic conditions and the 45m x 45m slab with Minneapolis MN climate.

The following runs used the final GTF coefficients and scalar constants. When the approximation for one input data set was used, the remaining inputs were held identical to those in Runs 1D and 2D.

#### GROUND SURFACE TEMPERATURE

Table 10 gives the numerical comparison of the data resulting from substituting the daily average outdoor air temperature for daily average ground surface temperature as the input at  $T_g$ . The error in total energy consumption over the entire cycle ranges from 17.1 % to 219.5 %. Inspection of

the graphical representation of the data (Figures 24, 25, 26, 27 and 28) reveals a common pattern in the error. In all cases, the largest factor in the error is a positive linear offset which is greatest in Phoenix where the temperature difference between the air temperature and ground temperature is highest. The larger slab, where the edge effect is less substantial, shows a much smaller effect of changing far field temperature.

#### DEEP GROUND TEMPERATURE

Table 11 and figures 29, 30, 31, 32 and 33 show the results of using the annual average outdoor air temperature as the deep ground temperature,  $T_d$ . Because the annual mean outdoor air temperature is less than the annual mean ground surface temperature, the calculated heat loss from the slab is correspondingly higher. Again, the largest component of the error is the linear offset. The error is small in moderate and cold climates -- less than 5%. In Phoenix there is only a slight difference between the annual mean outdoor air temperature and the indoor air temperature (0.1C) so that the annual mean heat flux through the slab is very small compared to other locations where the temperature difference is an order of magnitude larger. At the same time, the difference between the annual mean outdoor air temperature and the annual mean ground surface is much greater in Phoenix due for the most part to the increased solar gain. The consequence of these two conditions is a much greater effect from this substitution than is seen in the other climates. In general, however, it gives good results and even gives a slightly better fit in some cases

as evidenced by the increase in the percentage of the data within 15% of the FDM data for small slab in Medford and the larger slab in Minneapolis.

#### SLAB TEMPERATURE

In this case a constant value is substituted for the input data set. This is a convenient substitution and practical for the many cases where the slab temperature is, in fact, nearly constant. Table 12 and Figures 34, 35, 36 and 37 give the results of this substitution. In assuming a constant temperature approximately 10% higher than the actual floor surface temperature a error of roughly 10% is introduced. This error is primarily a linear shift, which appears typical of input data set changes. It seems to be due for the most part to the difference between the mean value of the original data set and the mean of the substituted data. As in all the other cases of input substitution, the effect is substantially smaller for the larger slab.

#### GENERAL COMMENTS

For the most part, the changes described in this section cause linear shifts of the flux curve. This linear shift appears to be related principally to the difference between the mean of the original data set and the mean of the substituted data. The slight changes in the shape of the input data curves do not have a great effect on the flux. It is probable, based on the linearity of the change, that altering more than one input would result in a linear shift related to the added effects of the individual changes.

Table 10: Results of Substituting Daily Average Outdoor Air Temperature for Daily Average Ground Surface Temperature

MODEL	LOCAT'N	EDGE SIZE [m]	MEAN FLUX [W/m <sup>2</sup> ]	% OF DATA WITHIN 15% OF FDM [%]	TOTAL ANNUAL ENERGY CONSUMP [kWhr]	% ERROR IN TOTAL ENERGY CONSUMP [%]	TOTAL ANNUAL DIFF IN ENERGY CONSUMP [kWhr]
FDM	Minn	12	6.13	-----	7716.9	-----	-----
GTF	Minn	12	8.11	21	10197.4	+24.3	+2480.5
FDM	Medford	12	3.87	-----	4867.1	-----	-----
GTF	Medford	12	6.30	17	7923.0	+62.8	+3055.9
FDM	Phila	12	3.89	-----	4893.7	-----	-----
GTF	Phila	12	5.65	12	7101.6	+45.1	+2207.9
FDM	Phoenix	12	-1.66	-----	-2082.9	-----	-----
GTF	Phoenix	12	1.98	2	2488.8	-219.5	+4571.7
FDM	Minn	45	2.50	-----	44167.7	-----	-----
GTF	Minn	45	2.92	47	51711.8	+17.1	+7544.1

Figure 24: Flux and Difference --  $T_f = T_{oa}$  -- Minneapolis MN

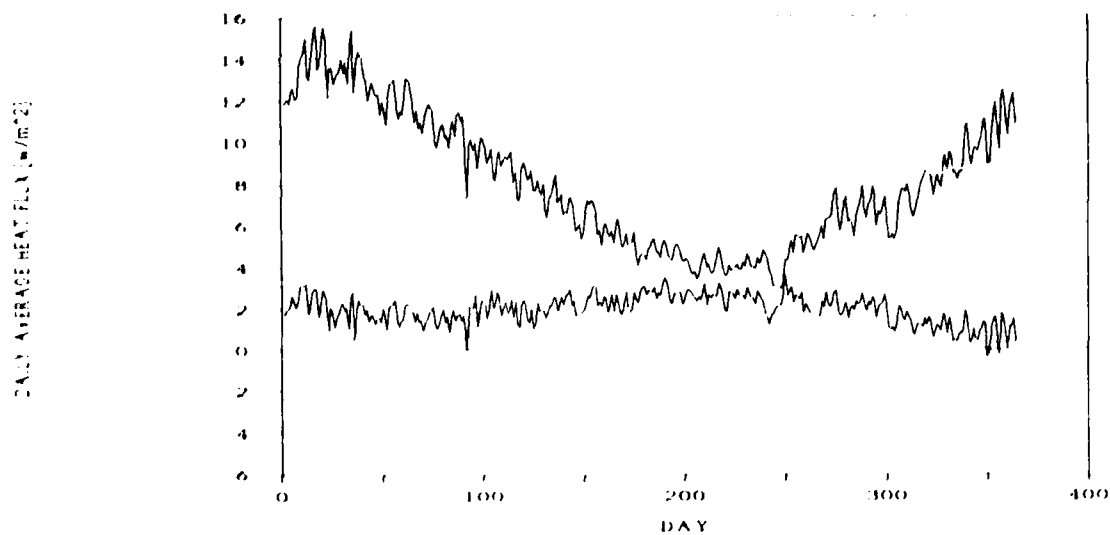


Figure 25: Flux and Difference --  $T_f = T_{oa}$  -- Medford OR

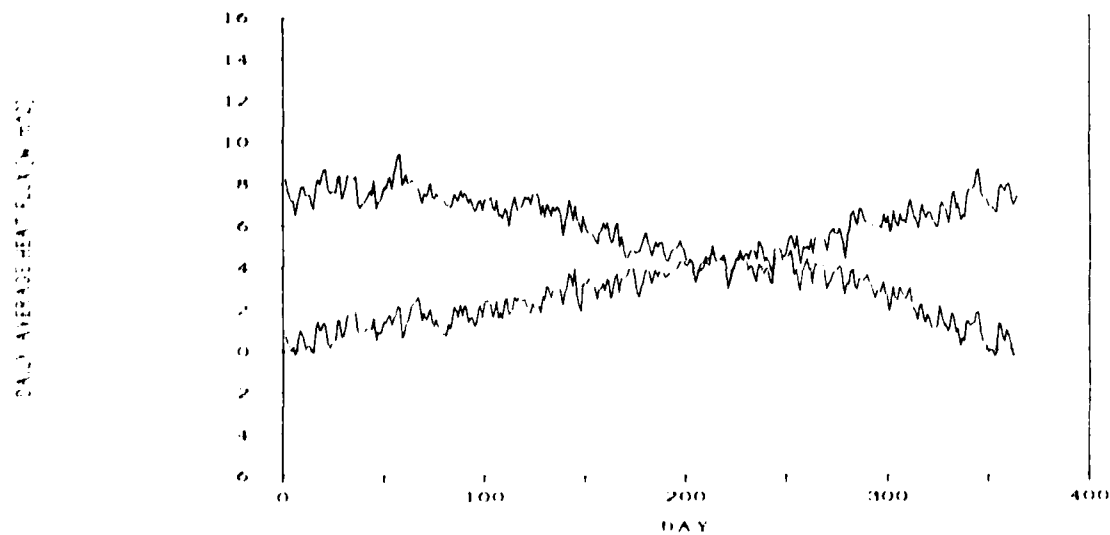


Figure 26: Flux and Difference --  $T_f - T_{oa}$  -- Philadelphia  
PA

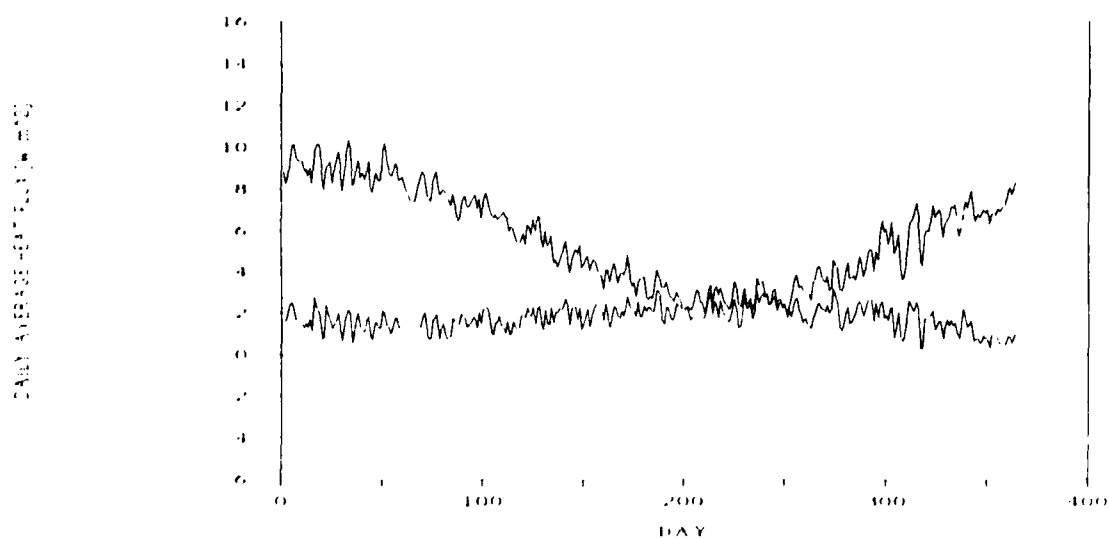


Figure 27: Flux and Difference --  $T_f - T_{oa}$  -- Phoenix AZ

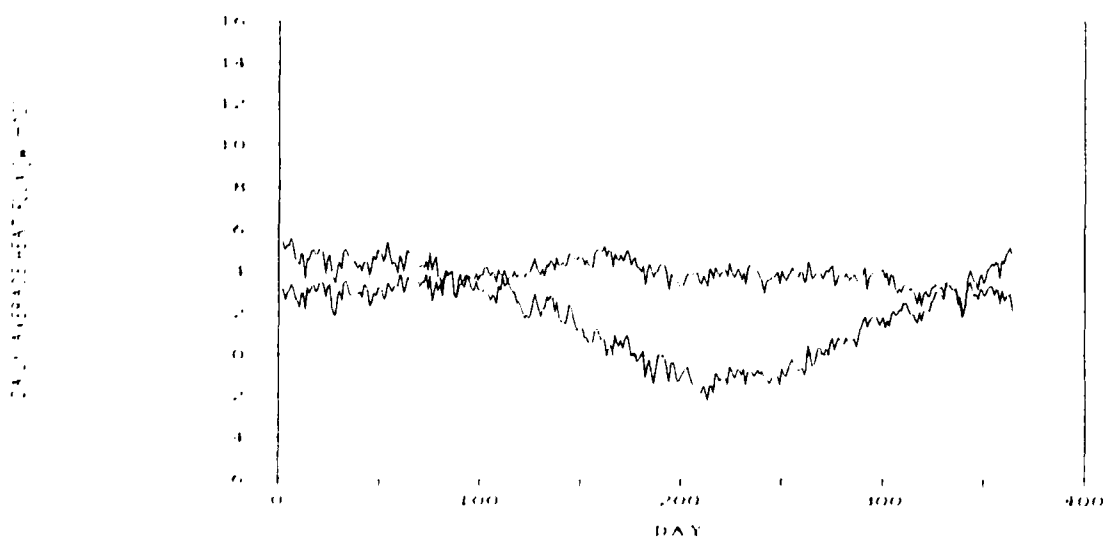


Figure 28: Flux and Difference --  $T_i - T_{oa}$  -- 45 x 45 --  
Minneapolis MN

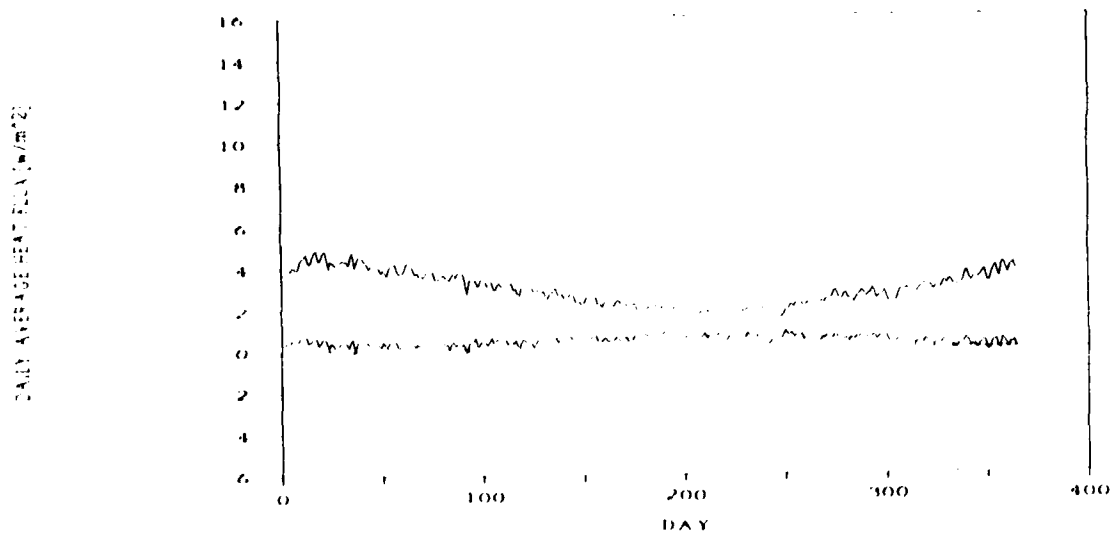


Table 11: Results of Substituting Annual Average Air Temperature for Annual Average Ground Surface Temperature

MODEL	LOCAT'N	EDGE SIZE [m]	MEAN FLUX [W/m <sup>2</sup> ]	% OF DATA WITHIN 15% OF FDM [%]	TOTAL ANNUAL ENERGY CONSUMP [kWhr]	% ERROR IN TOTAL ENERGY CONSUMP [%]	TOTAL ANNUAL DIFF IN ENERGY CONSUMP [kWhr]
FDM	Minn	12	6.13	-----	7716.9	-----	-----
GTF	Minn	12	6.32	87	7950.1	+2.9	+233.5
FDM	Medford	12	3.87	-----	4867.1	-----	-----
GTF	Medford	12	4.04	79	5083.7	+4.5	+216.6
FDM	Phila	12	3.89	-----	4893.7	-----	-----
GTF	Phila	12	3.99	78	5020.4	+2.6	+126.7
FDM	Phoenix	12	-1.66	-----	-2082.9	-----	-----
GTF	Phoenix	12	-1.03	12	-1299.7	-37.6	+783.2
FDM	Minn	45	2.50	-----	44167.7	-----	-----
GTF	Minn	45	2.51	100	44395.6	+0.5	+227.9

Figure 29: Flux and Difference --  $T_d = \text{Annual Mean } T_{oa}$  --  
Minneapolis MN

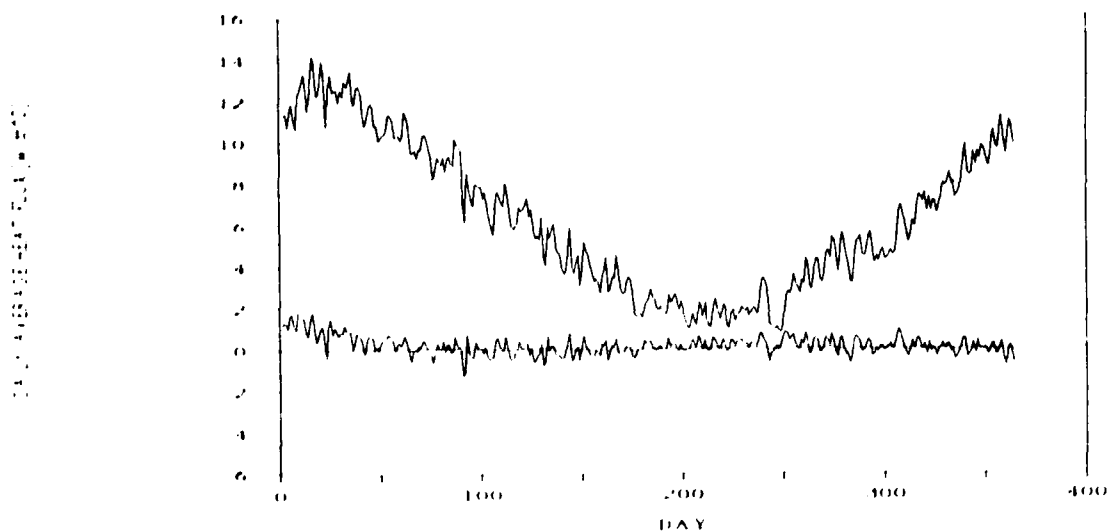


Figure 30: Flux and Difference --  $T_d = \text{Annual Mean } T_{oa}$  --  
Medford OR

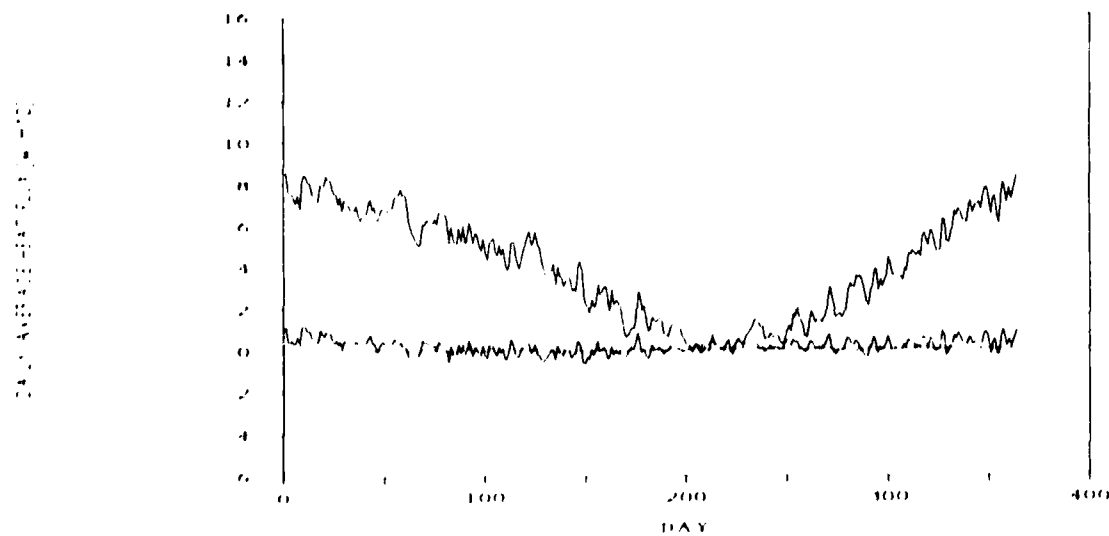


Figure 31: Flux and Difference --  $T_d = \text{Annual Mean } T_{oa}$  --  
Philadelphia PA

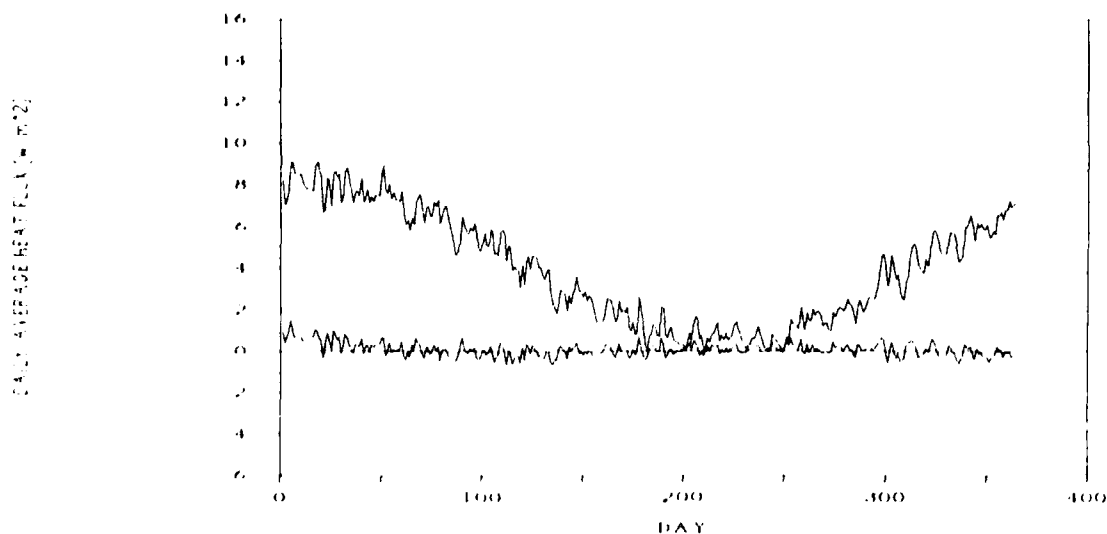


Figure 32: Flux and Difference --  $T_d = \text{Annual Mean } T_{oa}$  --  
Phoenix AZ

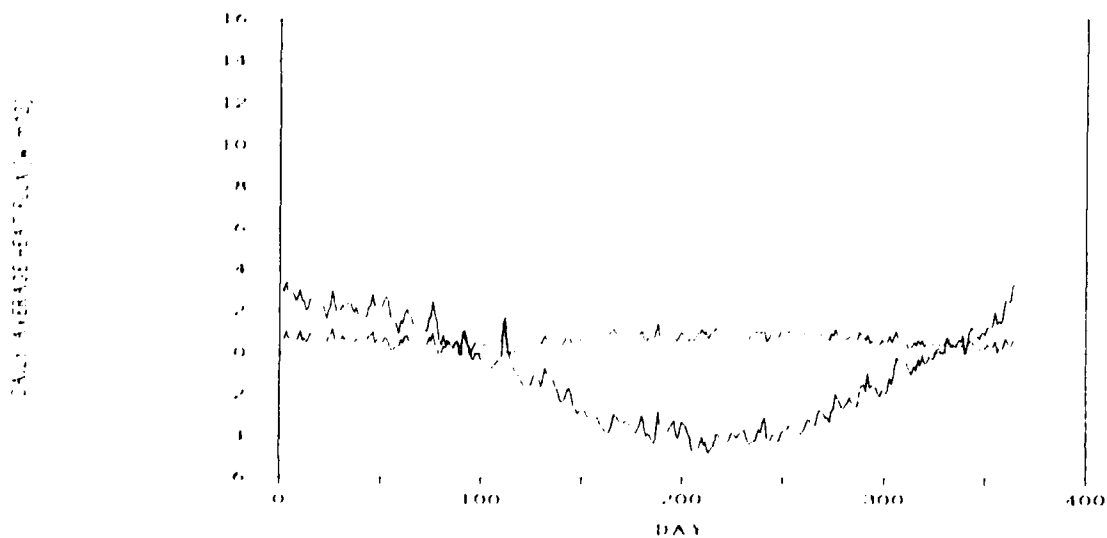


Figure 33: Flux and Difference --  $T_d = \text{Annual Mean } T_{oa}$  --  
45 x 45 -- Minneapolis MN

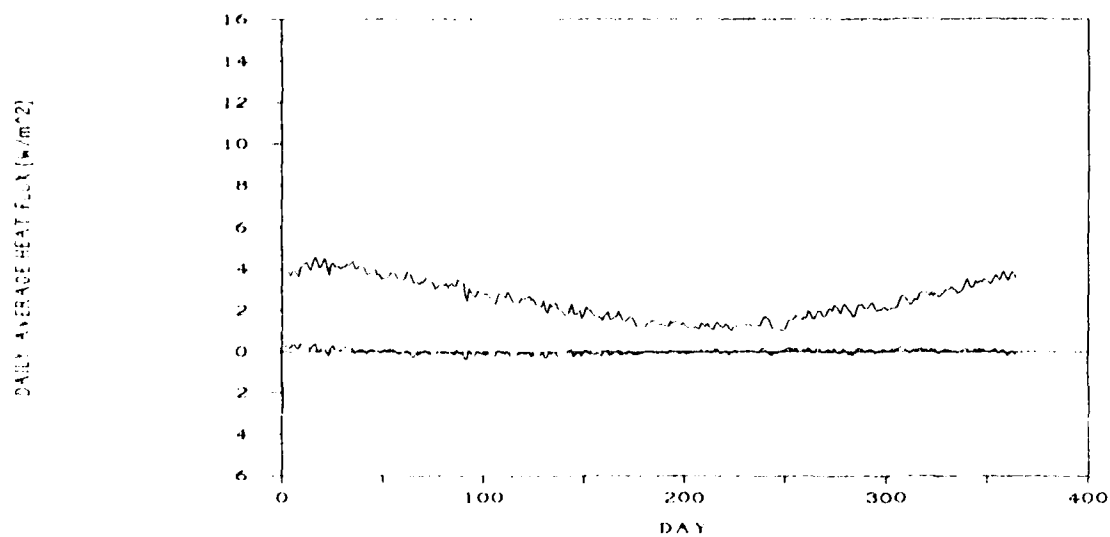


Table 12: Results of Substituting Constant Indoor Air Temperature for Daily Average Slab Surface Temperature

MODEL	LOCAT'N	EDGE SIZE [m]	MEAN FLUX [W/m <sup>2</sup> ]	% OF DATA WITHIN 15% OF FDM [%]	TOTAL ANNUAL ENERGY CONSUMP [kWhr]	% ERROR IN TOTAL ENERGY CONSUMP [%]	TOTAL ANNUAL DIFF IN ENERGY CONSUMP [kWhr]
FDM	Minn	12	6.13	-----	7716.9	-----	-----
GTF	Minn	12	6.74	63	8480.0	+9.0	+763.1
FDM	Medford	12	3.87	-----	4867.1	-----	-----
GTF	Medford	12	4.27	66	5967.6	+10.3	+1100.5
FDM	Phila	12	3.89	-----	4893.7	-----	-----
GTF	Phila	12	4.29	62	5398.7	+10.3	+505.0
FDM	Phoenix	12	-1.66	-----	-2082.9	-----	-----
GTF	Phoenix	12	-1.38	66	-1736.8	-16.6	+346.1
FDM	Minn	45	2.50	-----	44167.7	-----	-----
GTF	Minn	45	2.47	99	43725.3	-1.0	-442.4

Figure 34: Flux and Difference --  $T_b = T_{ia}$  -- Minneapolis MN

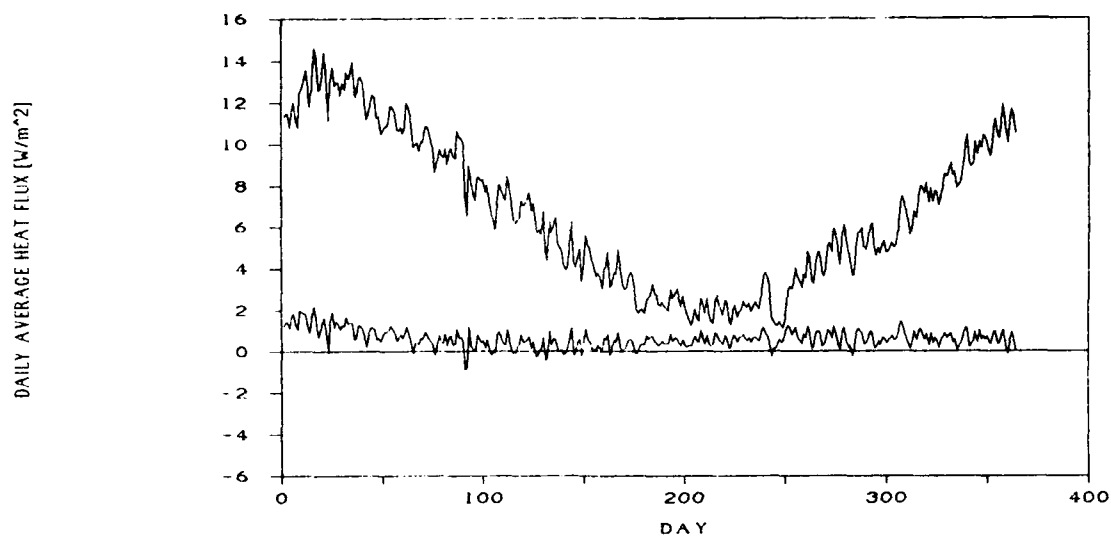


Figure 35: Flux and Difference --  $T_b = T_{ia}$  -- Medford OR

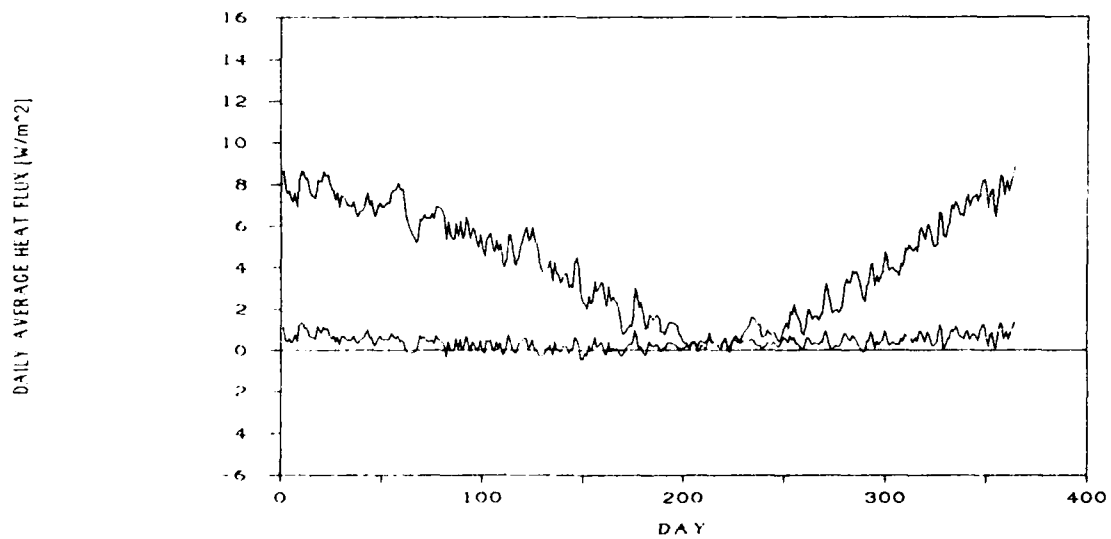


Figure 36: Flux and Difference --  $T_b = T_{ia}$  -- Philadelphia PA

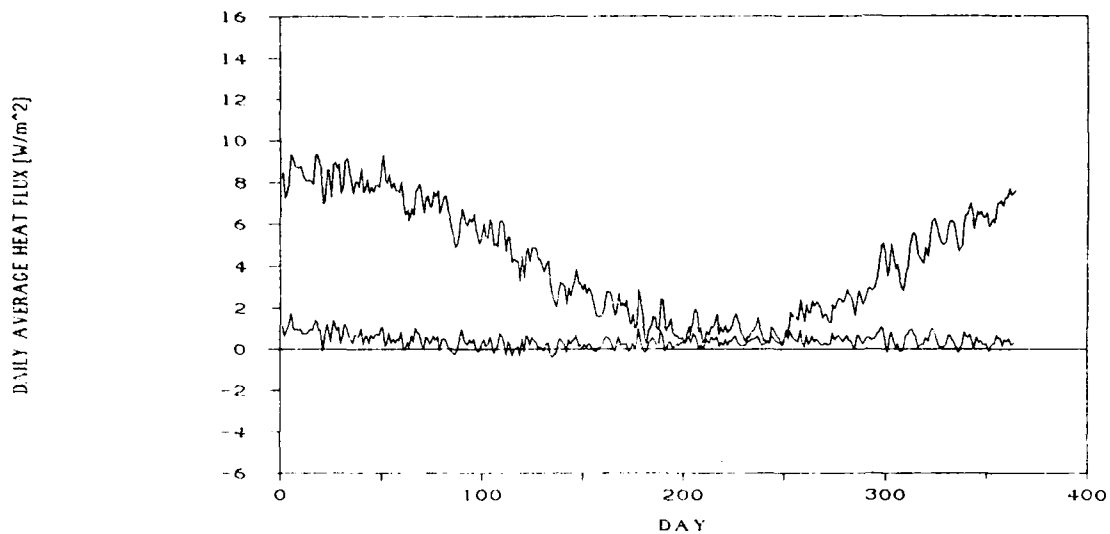


Figure 37: Flux and Difference --  $T_b = T_{ia}$  -- Phoenix AZ

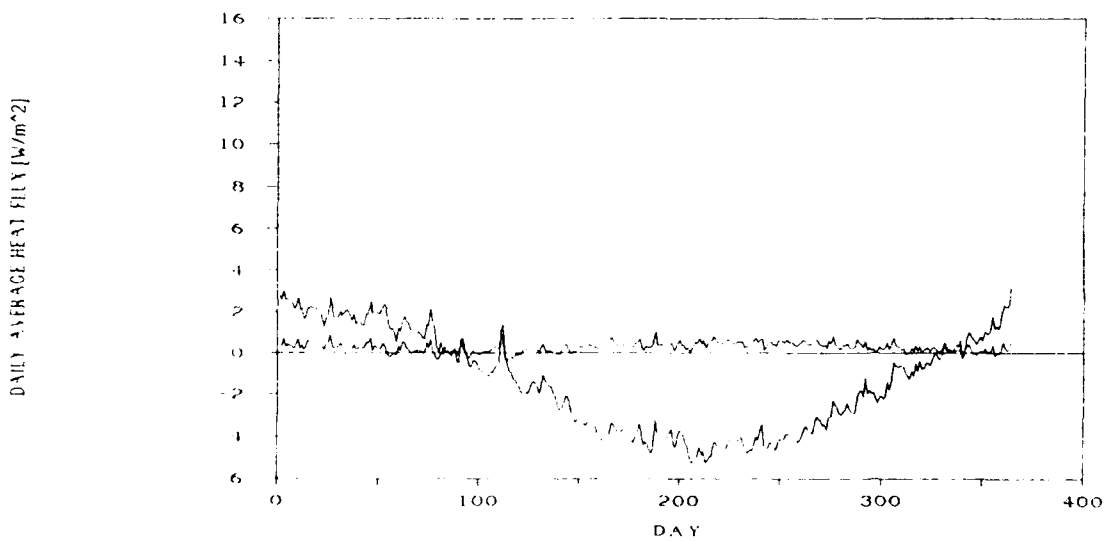
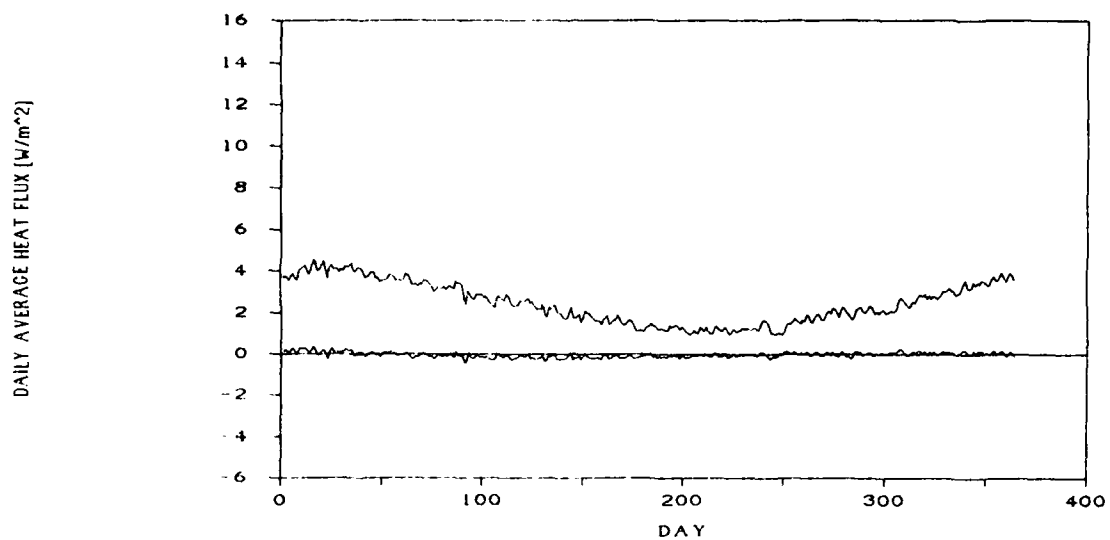


Figure 38: Flux and Difference --  $T_h = T_{in}$  -- 45 x 45 --  
Minneapolis MN



## 6 NETWORK PARAMETERS BASED ON CHARACTERISTIC LENGTH

Bahnfleth [3] reports that heat flux through slabs of several different rectangular geometries can be calculated based on the slab characteristic length ( $A/P$ ). This leads to the speculation that it may be possible to define the network parameters as functions of the soil geometry and slab characteristic length ( $A/P$ ), thereby allowing the use of the model with non-square slabs.

As a crude test of this proposition, empirical models were developed for slabs of four different configurations: 12m x 12m, 45m x 45m, 6m x 24m, and 18m x 112m. Little attempt was made at this point to attach geometric significance to the network parameters, but rather, each parameter set was adjusted based primarily on the quality of the resulting fit to each individual set of base case data. A parameter set was considered acceptable when more than 80% of the resulting data were within 15% of the corresponding FDM data and the error in total annual heat flux was less than 5% with the Minneapolis MN weather data. It should not be assumed that these parameter sets are in any way optimal. Once a set of parameters for each configuration was developed, the network parameters were compared in an effort to identify patterns among the four cases (see Table 13).

Several relationships became evident.  $A_{3f}$ ,  $A_{23}$ ,  $V_1$ , and  $V_2$  are of identical or similar value when the area of the slabs are (nearly) identical. This is a strong indication that those parameters are functions of the slab area. Correspondingly,  $A_{6a}$  and  $A_{2d}$  appear to be functions of the slab perimeter. The remaining parameters are assumed to be

functions of characteristic length, A/P. Pairing the two square slabs and the two non-square slabs, a line is fit to each set and the coefficients of the resulting equations compared. For equations of the form

$$y = a + bx \quad (114)$$

the coefficients and variables are shown in Table 14.

It is clear that a single set of linear equations for the network parameters in terms of the slab area, perimeter or characteristic length can be written and should give acceptable results for all four cases. A suggested set of equations, based on these data is shown in Table 15. Network parameters are calculated using these data and are shown in Table 16.

Using the original  $L$  matrix and the  $A$  and  $V$  matrices generated using Table 16, new GTFs and scalar constants are calculated and QCALC is used to calculate the daily average heat flux through the slab using Minneapolis MN climatological data. The results are shown in Figures 38, 39, 40, and 41. Numerical comparisons are given in Table 17. In all cases more than 80% of the data are within 15% of the FDM data, and the error in total energy consumption is less than 10%. It is evident that it is possible to develop a set of equations for calculating network parameters as functions of slab area, perimeter and characteristic length which give good results for a variety of rectangular geometries. The equations developed for this example should not be considered universal; a more rigorous method of parameter estima-

tion should be used to develop a truly generic parameter set. Nonetheless, this example indicates that such a procedure should yield good results.

Table 13 Parameter Sets for Empirical Models

	12x12	45x45	6x24	18x112
AREA [ $m^2$ ]	144	2025	144	2016
PERIMETER [m]	48	180	60	260
A/P [m]	3.00	11.25	2.4	7.75
% WITHIN 15% OF FDM	87	95	82	97
% ERROR IN TOTAL ENERGY CONSUMPTION	+3.3	-2.7	-0.6	-3.8
$A_{fe}$	157	608	121	415
$A_{12}$	493	1934	385	1322
$A_{be}$	200	650	255	1000
$A_{23}$	800	3000	792	3000
$A_{1b} = A_{1d}$	100	1881	90	1760
$A_{2d} = A_{2e}$	400	1500	600	2600
$A_{3f} = A_{3d}$	800	2000	878	2000
$V_1$	80	1000	80	1000
$V_2$	320	1850	320	2000
$V_3$	100	100	100	100

Table 14: Equations of Lines Fit to Empirical Data

PARAMETER	a		b		VARIABLE
	SQUARE	NONSQUARE	SQUARE	NONSQUARE	
$A_{fe}$	-7.0	-11	55	55	A/P
$A_{12}$	-31	-35	175	175	A/P
$A_{be}$	36	32	3.4	3.7	P
$A_{23}$	632	622	1.2	1.2	A
$A_{1b} = A_{1d}$	-36	-38	.95	.89	A/P
$A_{2d} = A_{2e}$	0	89	8.3	7.35	P
$A_{3f} = A_{3d}$	708	792	.64	.60	A
$V_1$	9.6	9.2	.49	.49	A
$V_2$	203	191	.81	.90	A
$V_3$	100	100	0	0	CONSTANT

Table 15: Equations of Common Lines Fit to Empirical Data

PARAMETER	a	b	VARIABLE
$A_{fe}$	-9.0	55	A/P
$A_{12}$	-33	175	A/P
$A_{be}$	34	3.6	P
$A_{23}$	627	1.2	A
$A_{1b} = A_{1d}$	-36	.9	A/P
$A_{2d} = A_{2e}$	0	9	P
$A_{3f} = A_{3d}$	750	.6	A
$V_1$	9.4	.5	A
$V_2$	203	.9	A
$V_3$	100	0	CONSTANT

Table 16: Parameter Sets Calculated Using Empirical Equations

	12x12	45x45	6x24	18x112
AREA [ $m^2$ ]	144	2025	144	2016
PERIMETER [m]	48	180	60	260
A/P [m]	3.00	11.25	2.4	7.75
$A_{fe}$	156	610	123	417
$A_{12}$	492	1936	387	1324
$A_{be}$	207	682	250	970
$A_{23}$	800	3057	800	3046
$A_{1b} = A_{1d}$	94	1787	94	1778
$A_{2d} = A_{2e}$	432	1620	540	2340
$A_{3f} = A_{3d}$	836	1965	836	1960
$V_1$	81	1022	81	1017
$V_2$	327	2020	327	2011
$V_3$	100	100	100	100

Figure 39: Flux and Difference -- Run 3A

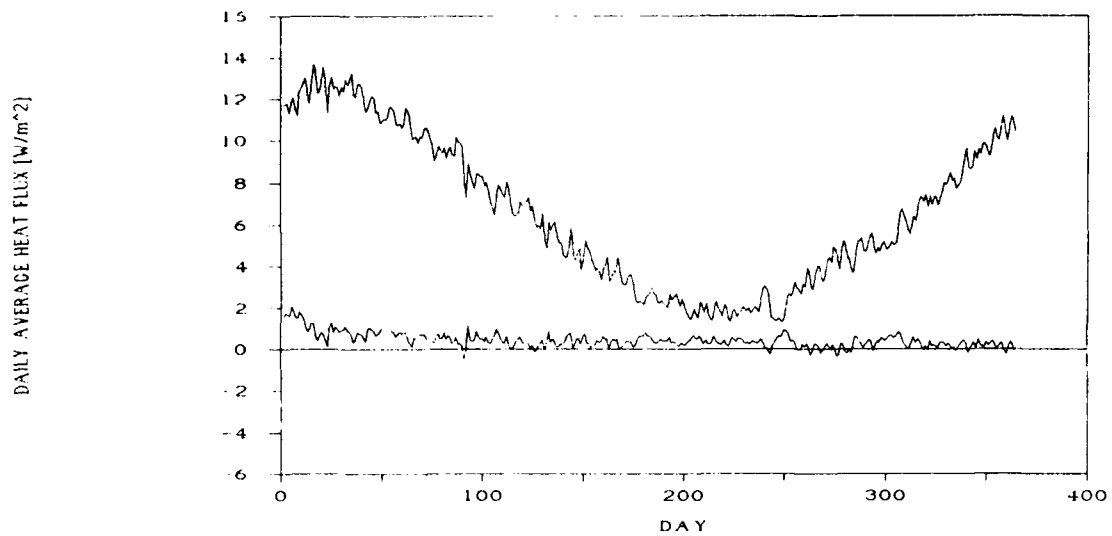


Figure 40: Flux and Difference -- Run 3B

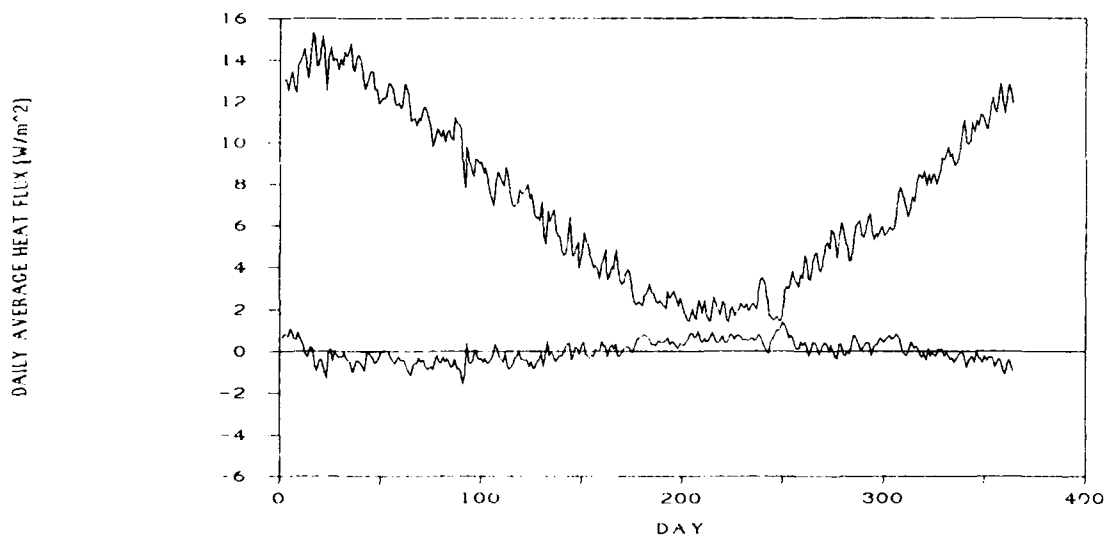


Figure 41: Flux and Difference -- Run 3C

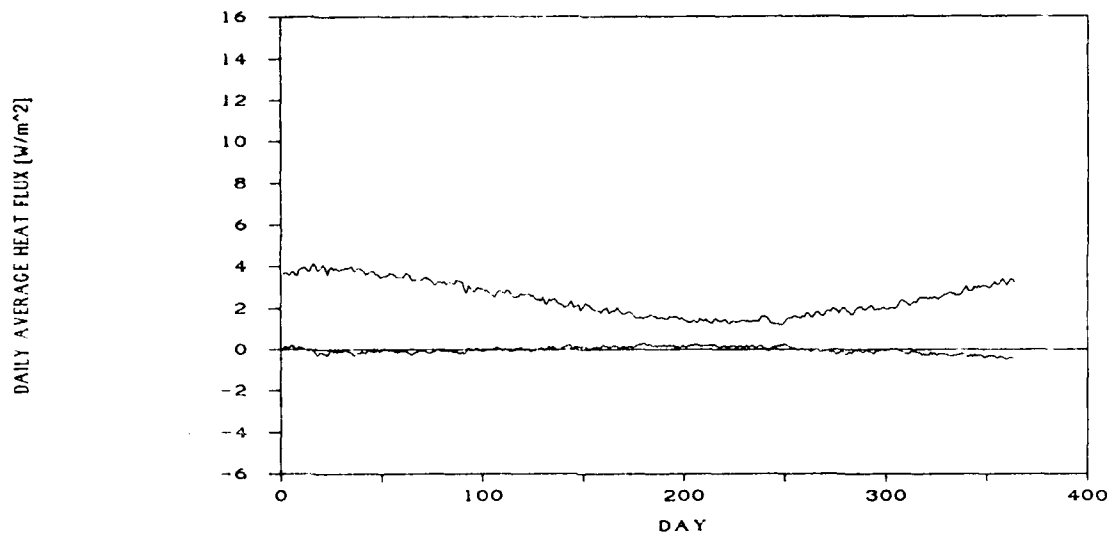


Figure 42: Flux and Difference -- Run 3D

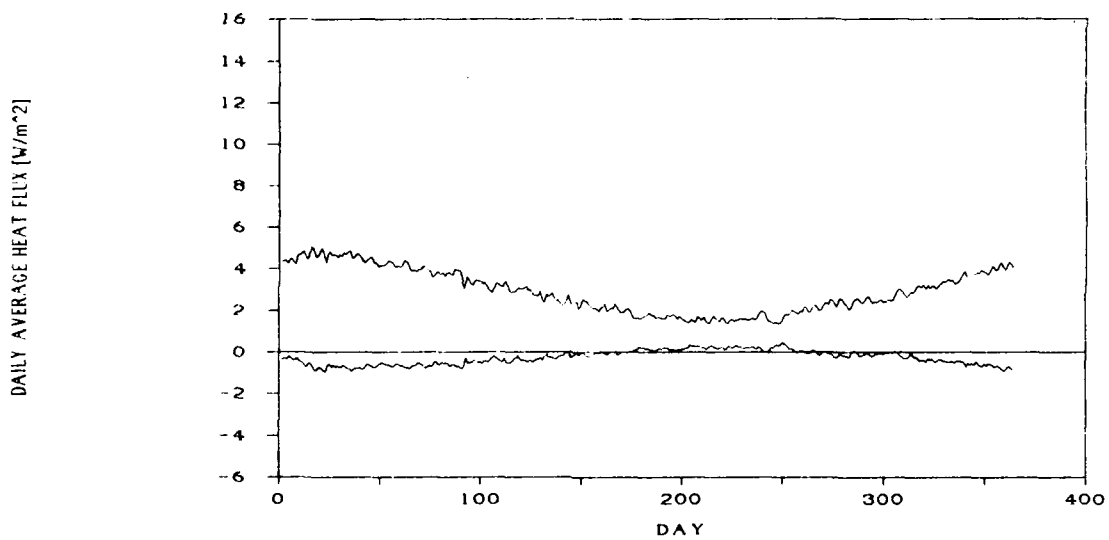


Table 17: Results of GTF Model Using Parameter Sets Based on Empirical Equations

MODEL	MEAN FLUX [W/m <sup>2</sup> ]	% OF DATA WITHIN 15% OF FDM [%]	TOTAL ANNUAL ENERGY CONSUMP [kWhr]	% ERROR IN TOTAL ENERGY CONSUMP [%]	TOTAL ANNUAL DIFF IN ENERGY CONSUMP [kWhr]
FDM-12x12	6.10	-----	7716.9	-----	-----
GTF-12x12	6.57	80	8263.1	+6.6	+546.2
FDM-6x24	7.30	-----	9180.2	-----	-----
GTF-6x24	7.31	81	9190.5	+0.1	+10.3
FDM-45x45	2.50	-----	44167.7	-----	-----
GTF-45x45	2.47	93	43763.6	-0.9	-404.1
FDM-18x112	3.19	-----	56405.2	-----	-----
GTF-18x112	2.93	86	51765.1	-8.2	-4640.1

## 7 UTILIZATION OF THE GTF MODEL FOR ENERGY ANALYSIS

Because of its conceptual similarity to existing energy analysis programs using transfer function models of building components, this model is particularly suitable for incorporation into these programs. When used with these types of hourly energy analysis programs, the ground network would be seen as another zone connected to the conditioned space by an "interzone partition" which would include the slab itself and the top 0.5m of soil. The surface inner and outer temperatures of the "partition" would be the calculated hourly slab surface temperature and the GTF model slab center and edge temperatures (which are equal in this case), respectively. An algorithm for the calculation of ground surface temperatures (such as TEARTH, developed by Bahnfleth) must be included in the processing of weather data in order to provide correct input values for the far-field and deep ground temperatures.

This model could also serve as part of a stand-alone slab heat loss program for situations where the daily average slab surface temperatures are known or can be reasonably approximated. For example, Section 5.2.4 showed that substituting a constant indoor air temperature in place of the slab surface temperature gave acceptable results for all locations and both slab sizes. The program would also require an algorithm for the calculation of undisturbed ground surface temperatures.

## 8 CONCLUSIONS

A simple multiple-input transfer function model of the heat transfer in the ground beneath a square slab was presented. It was tested and modified to model both relatively small slabs where edge effects are strong and larger slabs whose heat flux is more strongly effected by the flux through the core. Tested over a broad range of climatic conditions, the model calculates slab heat flux within  $1 \text{ W/m}^2$  at all times and for all locations. This translates to an error of less than 1% (as compared to the detailed finite difference model) for moderate and cold climates and 12% for Phoenix where the total flux is very low. The accuracy of the model is dependent upon the accuracy of the input data, however, some reasonable approximations to the necessary input data can give acceptable results.

The full capability of the model was not tested in this study. Further work to develop a definition of the network parameters based on characteristic length could expand the use of the model to non-square and possibly even non-rectangular surfaces. Testing, and if necessary, modification of the parameter equations to support differential slab core and slab edge temperatures would allow the model to be used more effectively for insulation studies where the placement of the insulation is contingent on the slab to environment temperature difference.

## 9 REFERENCES

1. Ceylan, H.T., and Myers, G.E., "Long-Time Solutions to Heat-Conduction Transients with Time-Dependent Inputs," ASME Journal of Heat Transfer, v. 102, Feb 1980.
2. Seem, J.E., MODELING OF HEAT TRANSFER IN BUILDINGS, Ph.D thesis, Univ of Wisconsin-Madison, 1987.
3. Bahnfleth, W.P., THREE-DIMENSIONAL MODELLING OF HEAT TRANSFER FROM SLAB FLOORS, Ph.D. thesis, Univ of Illinois at Champaign-Urbana, 1989.
4. Shipp, P.H., THERMAL CHARACTERISTICS OF LARGE EARTH-SHELTERED STRUCTURES, Ph.D. thesis, Univ of Minnesota, 1979.
5. Kusuda, T., and Bean, J.W., "Simplified Methods for Determining Seasonal Heat Loss from Uninsulated Slab-on-Grade Floors", ASHRAE Transactions, v. 90, Part 1b, 1984.

## APPENDIX A SEEM'S METHOD

### Seem's Method for Calculating Transfer Functions for Multidimensional Heat Transfer

The system is described by a series of equations in state space formulation:

$$\frac{\partial X}{\partial t} = AX + BU \quad (\text{A.1})$$

$$Q = CX + DU \quad (\text{A.2})$$

where

$X$  = vector of state variables

$U$  = vector of known input variables

$Q$  = vector of output variables.

The solution of this system of equations is:

$$X_{t+\delta} = e^{A\delta} X_t + \int_t^{t+\delta} e^{A(t+\delta-\tau)} B U(\tau) d\tau \quad (\text{A.3})$$

The input function of the form:

$$U(\tau) = U_t + \frac{\tau - t}{\delta} (U_{t+\delta} - U_t) \quad (\text{A.4})$$

is substituted into the solution equation and the integrals evaluated leaving the solution equation

$$X_{t+\delta} = \Phi X_t + (\Gamma_1 - \Gamma_2) U_t + \Gamma_2 U_{t+\delta} \quad (\text{A.5})$$

where

$\Phi = e^{\mathcal{A}\delta}$  = the exponential matrix

$$\Gamma_1 = \mathcal{A}^{-1} (e^{\mathcal{A}\delta} - I) \mathcal{B}$$

$$\Gamma_2 = \mathcal{A}^{-1} \left( \frac{\Gamma_1}{\delta} - \mathcal{B} \right)$$

The forward shift operator

$$F v_t = v_{t+\delta} \quad (\text{A.6})$$

which relates  $v_{t+\delta}$  to its previous values  $v_t$ , is used in the solution equation in order to cast the equation entirely in time  $t$ :

$$(FI - \Phi) X_t = (F\Gamma_2 + \Gamma_1 - \Gamma_2) U_t \quad (\text{A.7})$$

or

$$X_t = (FI - \Phi)^{-1} (F\Gamma_2 + \Gamma_1 - \Gamma_2) U_t.$$

This equation gives the state variables in terms of the inputs. It is substituted back into the state output equation to give the outputs in terms of the inputs:

$$Q_t = (C(FI - \Phi)^{-1}(F\Gamma_2 + \Gamma_1 - \Gamma_2) + \mathcal{D})U_t \quad (\text{A.8})$$

where

$$(FI - \Phi)^{-1} = \frac{R_0 F^{n-1} + R_1 F^{n-2} + \dots + R_{n-2} F + R_{n-1}}{F^n + e_1 F^{n-1} + \dots + e_{n-1} F + e_n}. \quad (\text{A.9})$$

Substituting, combining common terms of the forward shift operator,  $F$ , and shifting the equation  $n$  timesteps back leaves the transfer function equation

$$\begin{aligned} Q_t + e_1 Q_{t-b} + \dots + e_n Q_{t-nb} &= (C R_0 \Gamma_2 + \mathcal{D}) U_t \\ &+ (C(R_0(\Gamma_1 - \Gamma_2) + R_1 \Gamma_2) + e_1 \mathcal{D}) U_{t-b} \\ &+ (C(R_1(\Gamma_1 - \Gamma_2) + R_2 \Gamma_2) + e_2 \mathcal{D}) U_{t-2b} + \dots \\ &+ (C(R_{n-2}(\Gamma_1 - \Gamma_2) + R_{n-1} \Gamma_2) + e_{n-1} \mathcal{D}) U_{t-(n-1)b} \\ &+ (C R_{n-1}(\Gamma_1 - \Gamma_2) + e_n \mathcal{D}) U_{t-nb}. \end{aligned} \quad (\text{A.10})$$

More concisely,

$$Q_t = \sum_{j=0}^n (S_j U_{t-jb}) - \sum_{j=1}^n (e_j Q_{t-jb}) \quad (\text{A.11})$$

where

$$S_0 = C R_0 \Gamma_2 + \mathcal{D}$$

$$S_j = C(R_{j-1}(\Gamma_1 - \Gamma_2) + R_j \Gamma_2) + e_j \mathcal{D} \quad \text{for } 1 \leq j \leq n-1$$

$$S_n = C R_{n-1}(\Gamma_1 - \Gamma_2) + e_n \mathcal{D}$$

Seem's computationally efficient procedure for calculating numerically significant coefficients uses Leverrier's algorithm with the analytical solution as follows:

1. Calculate the exponential matrix by a truncated power series expansion with scaling and squaring

1.1 Calculate the matrix row norm of matrix  $A\delta$

$$|A\delta|_{\infty} = \max_{1 \leq i \leq n} \sum_{j=1}^n |a_{ij}\delta| \quad (\text{A.12})$$

1.2 Find the smallest integer  $k$  such that

$$2^k \geq |A\delta|_{\infty} \quad (\text{A.13})$$

1.3 Divide matrix  $A\delta$  by  $2^k$ .

1.4 Calculate the number of terms to keep

$$L = \min \{ (3|A\delta| + 6) \vee 100 \} \quad (\text{A.14})$$

1.5 Calculate  $e^{\frac{A\delta}{2^k}}$

$$e^{\frac{A\delta}{2^k}} = I + \frac{A\delta}{2^k} + \frac{\left(\frac{A\delta}{2^k}\right)^2}{2!} + \frac{\left(\frac{A\delta}{2^k}\right)^3}{3!} + \dots + \frac{\left(\frac{A\delta}{2^k}\right)^L}{L!} \quad (\text{A.15})$$

1.6 Calculate  $e^{A\delta}$

$$e^{A\delta} = e^{\left(\frac{A\delta}{2^k}\right)2^k} \quad (\text{A.16})$$

2. Calculate  $\Gamma_1$  and  $\Gamma_2$

$$\Gamma_1 = \mathcal{A}^{-1}(e^{\mathcal{A}\delta} - I)\mathcal{B} \quad (\text{A.17})$$

$$\Gamma_2 = \mathcal{A}^{-1}\left(\frac{\Gamma_1}{\delta} - \mathcal{B}\right)$$

3. Calculate the  $S_0$  matrix

$$S_0 = \mathcal{C} R_0 \Gamma_2 + \mathcal{D} \quad (\text{A.18})$$

4. Calculate the  $S$  matrices for  $1 \leq j \leq n-1$  where  $n$  is the number of state variables

4.1 Set starting  $R$  matrix to the identity matrix

$$R_{\text{new}} = I \quad (\text{A.19})$$

4.2 Calculate the scalar constant,  $e_j$  and the next  $R$  matrix,  $R_{\text{new}}$

$$R_{\text{old}} = R_{\text{new}} \quad (\text{A.20})$$

$$e_j = - \frac{\text{Trace}(\Phi R_{\text{old}})}{j}$$

$$R_{\text{new}} = \Phi R_{\text{old}} + e_j I$$

4.3 Calculate the next  $S$  matrix

$$S_j = \mathcal{C}(R_{\text{old}}(\Gamma_1 - \Gamma_2) + R_{\text{new}}\Gamma_2) + e_j \mathcal{D} \quad (\text{A.21})$$

4.4 Iterate 4.2 - 4.3 resetting  $j = j+1$  until  $j = n-1$

5. Calculate scalar constant and  $S$  matrix for  $j = n$

$$e_n = - \frac{\text{Trace}(\Phi R_{new})}{n} \quad (\text{A.22})$$

$$S_n = C R_{new}(\Gamma_1 - \Gamma_2) + e_n \mathcal{D}.$$

## APPENDIX B TRUE BASIC PROGRAM GTF

### TRUBASIC PROGRAM GTF FOR CALCULATING MULTIPLE INPUT GROUND TRANSFER FUNCTION COEFFICIENTS AND SCALAR CONSTANTS

```
RECORD,RECSIZE 64
INPUT PROMPT "RUN ID? ": runid$
OPEN #3: NAME "D:\TRUBASIC\INDATA\"&runid$&"GTFs",CREATE
NEWOLD,ORGANIZATION
SET #3: POINTER BEGIN
WRITE #3: DATE$,TIME$
WRITE #3: runid$
DIM CONDUCTIVITY(7,7),DENSITY(3),SPECIFIC_HT(3)
DIM AREA(7,7),LENGTH(7,7)
DIM P(4),H(7),AOV(7),VOLUME(3)
DIM DISTANCE(4)
DIM G(7,7),CINV(3),D(4,4),C(4,3),A(3,3),B(3,4)
DIM IDEN(3,3),PHIADJ(3,3),PHI(3,3),PHINEW(3,3),FACTOR(3,3)
DIM ADEL(7,7),AADJ(7,7)
DIM GAMMA1(3,3),GAMMA2(3,3),AINV(3,3),TEMP1(4,4),TEMP2(4,4)
DIM ROLD(10,10),RNEW(10,10),SOLD(10,10),SNEW(10,10),SFINAL(1
0,10)
DIM TABLE(4,4)

CALL PROPERTIES

CALL MODEL

REM   Generic Equation Construction
REM   set up equation matrices
```

```

REM    set up general configuration
REM    for model with 3 state variables and 4 inputs
REM

LET num_state_var=3
LET num_inputs=4

REM
REM    Generate thermal resistance matrix G with equation
REM           $G(i,j) = k(i,j) * A(i,j) / L(i,j)$ 
REM
REM
MAT G=ZER
FOR i=1 to num_state_var + num_inputs
    FOR j=1 to num_state_var + num_inputs
        IF LENGTH(i,j)=0 THEN
            LET G(i,j)=0
        ELSE
            LET G(i,j)=CONDUCTIVITY(i,j)*AREA(i,j)/LENGTH(i,j)
        END IF
    NEXT j
NEXT i

REM
REM    Generate the matrix of the inverses of the thermal
capacitances
REM     $CINV(i) = (DENSITY(i) * SPECIFIC\_HT(i) * VOLUME(i))^{(-1)}$ 
REM
REM
FOR i=1 to num_state_var
    LET CINV(i)=(DENSITY(i)*SPECIFIC_HT(i)*VOLUME(i))^{(-1)}
NEXT i

```

```

REM
REM   Generate the coefficient matrices
REM
REM
REM
REM           COEFFICIENT MATRICES OF THE BASIC EQUATIONS
REM
REM            $\frac{dX}{dT} = A \cdot x + B \cdot u$ 
REM
REM            $Q = C \cdot x + D \cdot u$ 
REM
REM           where  $x$  is the vector of state variables and
REM            $u$  is the vector of inputs
REM
REM   Matrix A
REM
FOR i=1 to num_state_var
  FOR j=1 to num_state_var
    LET A(i,j)=G(i,j)*CINV(i)
  NEXT j
  FOR k=1 to num_state_var + num_inputs
    LET A(i,i) = A(i,i) - G(i,k)*CINV(i)
  NEXT k
NEXT i

REM   Matrices B and C
REM
FOR i=1 to num_state_var
  FOR j=1 to num_inputs
    LET B(i,j)=G(i,j+num_state_var)*CINV(i)
  
```

```

        LET C(j,i)=G(i,j+num_state_var)
    NEXT j
NEXT i

REM   Matrix D

FOR i=1 to num_inputs
    FOR j=1 to num_inputs
        LET D(i,j)=G(i+num_state_var,j+num_state_var)
    NEXT j
    FOR k=1 to num_state_var + num_inputs
        LET D(i,i)=D(i,i)-G(i+num_state_var,k)
    NEXT k
NEXT i

CALL TF
CALL STEADY_STATE_SOLN

SUB TF
REM Calculation of Transfer Function

CALL CALCPHI
CALL CALCGAMMAS
CALL CALCSCOEFF
END SUB

SUB CALCPHI
REM   Calculate exponential matrix PHI
REM   del=size of time step=1 hour

```

```

LET del=1.0
MAT ADEL=del*A

REM   Calculate the matrix row norm

FOR i = 1 to num_state_var
  LET test=0
  FOR j=1 to num_state_var
    LET test = test + ABS(ADEL(i,j))
  NEXT j
  LET matrix_row_norm=MAX(matrix_row_norm,test)
NEXT i

REM   Find the smallest integer such that 2^integer is
greater than or equal to
REM   the matrix row norm

DO WHILE 2^count<matrix_row_norm
  LET count=count+1
LOOP

REM   Divide matrix ADEL by 2^integer

MAT AADJ=(2^(-count))*ADEL

REM   Calculate matrix row norm for adjusted ADEL matrix,
AADJ

FOR i=1 to num_state_var
  LET test=0
  FOR j=1 to num_state_var
    LET test = test + ABS(AADJ(i,j))

```

```

    NEXT j
    LET aadj_matrix_row_norm=MAX(aadj_matrix_row_norm,test)
NEXT i

REM   Calculate number of terms to keep

LET how_far=MIN(((3*adj_matrix_row_norm)+6),100)

REM   Calculate the exponential of the adjusted matrix, AADJ

MAT IDEN=IDN(num_state_var)
LET num=2
MAT PHIADJ=ZER(UBOUND(A,1),UBOUND(A,2))

DO WHILE num<=how_far
    LET factorial =1
    FOR i=num to 1 STEP -1
        LET factorial=factorial*i
    NEXT i
    LET factora=(1/factorial)
    MAT FACTOR=factora*AADJ
    FOR j=1 to num-1
        MAT FACTOR=FACTOR*AADJ
    NEXT j
    MAT PHIADJ=FACTOR+PHIADJ
    LET num=num+1
LOOP

MAT PHIADJ=AADJ+PHIADJ
MAT PHIADJ=IDEN+PHIADJ

REM   Calculate exponential of matrix ADEL from exponential
of matrix AADJ

```

```

FOR i=1 to count
  MAT PHINEW=PHIADJ*PHIADJ
NEXT i

IF count=0 THEN
  MAT PHI=PHIADJ
ELSE
  MAT PHI=PHINEW
END IF

END SUB

SUB CALCGAMMAS
REM Calculate GAMMA1 and GAMMA2

MAT AINV=INV(A)
LET determinant=DET

MAT TEMP1=PHI-IDEN
MAT TEMP1=AINV*TEMP1
MAT GAMMA1=TEMP1*B
MAT TEMP1=(1/DEL)*GAMMA1
MAT TEMP1=TEMP1-B
MAT GAMMA2=AINV*TEMP1
END SUB

SUB CALCSCOEFF

```

```

MAT TEMP1=IDEN*GAMMA2
MAT TEMP1=C*TEMP1
MAT SOLD=TEMP1+D

MAT WRITE #3:SOLD

MAT TABLE=zer(num_inputs,num_inputs)
MAT TABLE=SOLD
MAT RNEW=IDEN

FOR i=1 to num_state_var
  MAT ROLD=RNEW
  MAT TEMP1=PHI*ROLD
  LET trace = 0
  FOR j=1 to num_state_var
    LET trace=trace+TEMP1(j,j)
  NEXT j
  LET e=-trace/i

WRITE #3: e

  MAT TEMP1=PHI*ROLD
  MAT TEMP2=e*IDEN
  MAT RNEW=TEMP1+TEMP2
  MAT TEMP1=GAMMA1-GAMMA2
  MAT TEMP1=ROLD*TEMP1
  MAT TEMP2=RNEW*GAMMA2
  MAT TEMP1=TEMP1+TEMP2
  MAT TEMP1=C*TEMP1
  MAT TEMP2=e*D
  MAT SNEW=TEMP1+TEMP2

MAT WRITE #3: SNEW

```

NEXT i

END SUB

SUB PROPERTIES

REM Assignment of soil properties

MAT CONDUCTIVITY = 8.640e4

!J/day-m-K

MAT DENSITY = 1200

!kg/m<sup>3</sup>

MAT SPECIFIC\_HT = 1200

!J/kg-K

END SUB

SUB MODEL

REM Surface Description

REM Square Surface

LET surface\_length=12

LET area\_of\_surface=surface\_length<sup>2</sup> !m<sup>2</sup>

LET perimeter\_of\_surface=4\*surface\_length !m

LET cl=area\_of\_surface/perimeter\_of\_surface

LET DISTANCE(1)=3.5 !m

LET DISTANCE(2)=14.5 !distance to deep ground temp m

LET DISTANCE(3)=12.5 !distance to far field temp m

LET DISTANCE(4)=perimeter\_of\_surface/(2\*pi) !distance  
center to edge m

REM Model

REM Basic Geometry

```

LET P(1)=2*pi*(1.0)/log(DISTANCE(4)/(DISTANCE(4)-1.0))
LET P(2)=P(1)
LET P(3)=2*pi*4.5*c1
LET P(4)=P(3)

LET H(1)=DISTANCE(1)
LET H(2)=DISTANCE(2)-h(1)
LET H(3)=h(1)
LET H(4)=DISTANCE(2)-h(3)
LET H(5)=DISTANCE(2)/2
LET H(6)=1.0
LET H(7)=0.1

LET AOV(1)=P(1)*H(1)
LET AOV(2)=P(2)*H(2)
LET AOV(3)=P(3)*H(3)
LET AOV(4)=P(4)*H(4)
LET AOV(5)=pi*((area_of_surface/pi)^0.5-1.0)^2
LET AOV(6)=pi*((area_of_surface/pi)^0.5+2.5+0.15*c1)^2-
AOV(5)
LET AOV(7)=pi*((area_of_surface/pi)^0.5+DISTANCE(3))^2 -
AOV(6) - AOV(5)

LET VOLUME(1)=AOV(5)*H(5)
LET VOLUME(2)=AOV(6)*H(6)
LET VOLUME(3)=AOV(7)*H(7)

REM Set up basic geometry MATRICES

MAT AREA=ZER
LET AREA(1,2),AREA(2,1)=AOV(2)
LET AREA(1,4),AREA(4,1)=AOV(5)
LET AREA(1,6),AREA(6,1)=AOV(5)

```

```

LET AREA(2,3),AREA(3,2)=AOV(4)
LET AREA(2,6),AREA(6,2)=AOV(6)
LET AREA(2,7),AREA(7,2)=AOV(6)
LET AREA(3,5),AREA(5,3)=AOV(7)
LET AREA(3,6),AREA(6,3)=AOV(7)
LET AREA(4,7),AREA(7,4)=AOV(1)
LET AREA(5,7),AREA(7,5)=AOV(3)

MAT LENGTH=ZER
LET LENGTH(1,2),LENGTH(2,1),LENGTH(4,7),LENGTH(7,4) -
=DISTANCE(4)
LET LENGTH(1,4),LENGTH(4,1),LENGTH(2,7),LENGTH(7,2),LENGTH(3
,5),LENGTH(5,3)=DISTANCE(1)
LET LENGTH(1,6),LENGTH(6,1),LENGTH(2,6),LENGTH(6,2),LENGTH(3
,6),LENGTH(6,3)=DISTANCE(2)-DISTANCE(1)
LET LENGTH(2,3),LENGTH(3,2),LENGTH(5,7),LENGTH(7,5) -
=DISTANCE(3)

END SUB

SUB STEADY_STATE_SOLN

REM   Calculate the steady-state solution

DIM X(3,1),CBA(4,4),GG(4,4),T(4,1),Q(4,1)

MAT AINV=INV(A)

MAT X=AINV*B

MAT CBA=C*X

```

MAT GG=D-CBA

MAT GG=(1/(3600\*24))\*GG

MAT WRITE #3: GG

END SUB

END

## APPENDIX C TRUBASIC PROGRAM QCALC

TRUE BASIC PROGRAM QCALC  
FOR USING MULTIPLE-INPUT GROUND TRANSFER FUNCTIONS  
AND SCALAR CONSTANTS TO CALCULATE HEAT FLUX

```
INPUT PROMPT "GTF run id? ":gtfrunid$
INPUT PROMPT "LOCATION run id? ":locid$
INPUT PROMPT "RUN NUMBER id? ":numid$
INPUT PROMPT "Number of timesteps to calculate?":endtime

LET runid$=locid$&numid$
LET outname$=gtfrunid$&runid$&"OUT"
OPEN #3:NAME
"D:\TRUBASIC\INDATA\"&gttfrunid$&"GTFS",ORGANIZATION
RECORD,RECSIZE 64
OPEN #4:NAME "D:\TRUBASIC\INDATA\"&locid$&"GSTEMP",CREATE
NEWOLD,ORGANIZATION RECORD,RECSIZE 64
OPEN #5:NAME "D:\TRUBASIC\DATA\"&outname$,CREATE NEWOLD,OR-
GANIZATION RECORD,RECSIZE 64
SET #5:POINTER BEGIN
OPEN #9:NAME
"D:\TRUBASIC\INDATA\"&locid$&"BTEMP",ORGANIZATION
RECORD,RECSIZE 64
RESET #9:BEGIN
READ #3:gtfrundate$,gtfruntime$,gtfrunid$
DIM S0(4,4),S1(4,4),S2(4,4),S3(4,4),E(0 TO 3)
DIM SSTF(4,4)
DIM QSTART(4),TSTART(4)
DIM Q(4,0 TO 3),T(4,0 TO 3)
```

```

DIM Q0(4),T0(4),QSAVE(4)
DIM FACTOR0(4,0 TO 3),FACTOR1(4,0 TO 3),FACTOR2(4,0 TO
3),FACTOR3(4,0 TO 3),FACTORE(0 TO 4)
DIM QDIFF(4),QCONV(4,0 TO 3),PDIFF(4),QDIFFCONV(4)

WRITE #5: outname$,gtfrunid$

WRITE #5:endtime

REM  Initialize variables

LET E(0)=0.0
LET num_inputs=4
LET num_state_var=3
LET iteration =0
LET er=0.001
LET timestep=0

REM  Read in Multiple-input GTF coefficients and scalar con-
stants

MAT READ #3:S0
READ #3: E(1)

MAT READ #3: S1
READ #3: E(2)

MAT READ #3: S2
READ #3: E(3)

MAT READ #3: S3
MAT READ #3: SSTF

```

```

REM   Set up starting temperture and flux matrices

RESET #4: RECORD 2
READ #4:TSTART(2)
READ #9:TSTART(1)
RESET #9:BEGIN
INPUT PROMPT "DEEP GROUND TEMP [K]: ":TSTART(3)
LET TSTART(4)=TSTART(1)
RESET #4:RECORD 2
MAT QSTART=SSTF*TSTART
MAT QSAVE=ZER
FOR inp=1 to num_inputs
FOR hr=0 to num_state_var
    LET Q(inp,hr)=QSTART(inp)
    LET T(inp,hr)=TSTART(inp)
NEXT hr
NEXT inp
MAT Q=(3600*24)*Q

DO

REM   If system is not yet initialized, initialize system

    IF timestep=0 THEN
        CALL INITLOOP
        LET timestep=timestep+1
    END IF
    IF timestep=1 THEN
        RESET #4:RECORD 2
    END IF
    CALL CALCQ
    LET timestep=timestep+1
LOOP UNTIL timestep=>endtime

```

SUB INITLOOP

REM Initialize system by iterating on first 30 days of data

DO

RESET #4:RECORD 2

LET iteration=iteration+1

FOR in=1 to num\_inputs

LET QDIFF(in)=Q(in,0)-QSAVE(in)

IF QSAVE(in)<>0.0 THEN

LET PDIFF(in)=(QDIFF(in)/(ABS(QSAVE(in))))\*100

END IF

LET QSAVE(in)=Q(in,0)

NEXT in

LET cycle=0

DO WHILE cycle<=30

LET cycle=cycle+1

MAT QDIFFCONV=(1/(3600\*24))\*QDIFF

FOR inp =1 to num\_inputs

FOR hour=num\_state\_var-1 to 0 step -1

LET Q(inp,hour+1)=Q(inp,hour)

LET T(inp,hour+1)=T(inp,hour)

NEXT hour

NEXT inp

IF END #4 THEN

RESET #4:record 2

END IF

IF END #9 THEN

RESET #9:BEGIN

END IF

READ #4: T(2,0)

LET T(3,0)=TSTART(3)

REM Set slab edge temperature = slab center temperature

LET TSTART(4)=TSTART(1)

CALL CALCQ

LET T0(1)=T(1,0)

LET T0(2)=T(2,0)

LET T0(3)=T(3,0)

LET T0(4)=T(4,0)

LET Q0(1)=Q(1,0)

LET Q0(2)=Q(2,0)

LET Q0(3)=Q(3,0)

LET Q0(4)=Q(4,0)

MAT Q0=(1/(3600\*24))\*Q0

LOOP

REM If system does not initialize in 200 iterations, terminate initialization

IF iteration > 200 THEN

EXIT DO

END IF

LOOP UNTIL ABS(PDIFF(1))<er AND ABS(PDIFF(2))<er AND  
ABS(PDIFF(3))<er AND ABS(PDIFF(4))<er AND iteration>5  
END SUB

SUB CALCQ

IF timestep>0 THEN

FOR inp =1 to num\_inputs

FOR hour=num\_state\_var-1 to 0 step -1

LET Q(inp, hour+1)=Q(inp, hour)

LET T(inp, hour+1)=T(inp, hour)

NEXT hour

```

        LET Q(inp,0)=0.0
NEXT inp
    IF END #4 THEN
        RESET #4:record 2
    END IF
    IF END #9 THEN
        RESET #9:BEGIN
    END IF
    READ #4: T(2,0)
    LET T(3,0)=TSTART(3)
    READ #9: T(1,0)
    LET TSTART(4)=TSTART(1)
END IF

MAT FACTOR0=S0*T
MAT FACTOR1=S1*T
MAT FACTOR2=S2*T
MAT FACTOR3=S3*T
LET factor_format$ = "-#.#####^ ^ ^ ^ "
LET qsum=0.0

FOR L=1 TO 4
    LET FACTORE(L)=E(1)*Q(L,1)+E(2)*Q(L,2)+E(3)*Q(L,3)
    LET Q(L,0)=FACTOR0(L,0)+FACTOR1(L,1)+FACTOR2(L,2)+FACTOR3
    (L,3)-FACTORE(L)
    LET qsum=qsum+Q(L,0)
NEXT L

MAT QCONV = (1/(3600*24))*Q
LET qsumconv=(1/(3600*24))*QSUM

```

```
IF timestep=0 THEN
  LET q_format$="-#.#####^ ^ ^ ^  "
ELSE
  WRITE #5:QCONV(1,0),QCONV(2,0),QCONV(3,0),QCONV(4,0)
END IF

END SUB

END
```

## DISTRIBUTION

Chief of Engineers

ATTN: CEMP-C

ATTN: CEIM-SL (2)

ATTN: CERD-L

US Army Engineer Districts

ATTN: Engineering Div (41)

US Army Engineer Divisions

ATTN: Engineering Div (14)

US Military Academy 10996

ATTN: Dept of Geography & Computer Science

Harry Diamond Laboratories 20783

ATTN: Library

Fort Belvoir, VA 22060

ATTN: Engr Studies Center

CECRL

ATTN: Library 03755

CEWES

ATTN: Library 39180

NCEL 93043

ATTN: Library (Code L08A)

Engineering Societies Library

New York, NY 10017

National Institute of Standards and Tech 20899

Defense Technical Info Center 22314

ATTN: DDA (2)